INFLUENCE OF TEMPERATURE AND pH ON CORROSION RESISTANCE OF Ni–Cr AND Co–Cr DENTAL ALLOYS ON ORAL ENVIRONMENT

TBRAH NUOH KHALIFA SALEH

A thesis submitted in fulfillment of the requirements for the degree

Magister of Technology: Biomedical Technology

In the Faculty of Health and Wellness Sciences

At the Cape Peninsula University of Technology

Supervisor: Prof. Dherendra Gihwala

Co-supervisor: Prof. Malik Maaza

Bellville, South Africa

June 2015

DECLARATION

I, **Tbrah Nuoh Khalifa Saleh**, declare that the contents of this dissertation/thesis represent my own unaided work, and that the dissertation/thesis has not previously been submitted for academic examination towards any qualification. Furthermore, it represents my own opinions and not necessarily those of the Cape Peninsula University of Technology.

Signed: Date:

ABSTRACT

Dental alloys are widely used in direct contact with oral tissue. In recent years after the price of gold significantly increased, cheaper dental materials were generally considered in the market particularly dental alloys such as cobalt-chromium (Co–Cr), nickel-chromium (Ni–Cr) and titanium alloys. Cobalt–chromium alloys for example, are used in prosthetic for the fabrication of removable partial dentures and also for the fabrication of some fixed prosthetic appliances, due to its excellent properties such as biocompatibility, good mechanical behavior and corrosion resistant. In this work, the corrosion behavior of three different dental alloys, namely PD CASTA H, CERACAST NB Beryllium Free and PD 2000 alloys were studied and tested in Ringers solution (artificial saliva) at different pH values and temperature. The dental alloys were immersed in the Ringers solution for 14 days. The microstructure characterization and composition of selected alloys were done before and after 14 days of corrosion test on artificial saliva, using scanning electron microscopy (SEM). The surface roughness of the alloys was investigated by atomic force microscopy (AFM). The EDS, XRD, and TOF–SIMS were also used in the study. Electrochemical measurement on dental alloys was performed using cyclic voltammetry (CV). A saturated calomel electrode (SCE) was used as reference electrode, platinum was used as counter-electrode and Ni–Cr and Co–Cr alloys were used as working electrode. The polarization curves were plotted in the potential range of -1000 mV/SCE to +1000 mV/SCE at scanning rate of 0.2 mVs^{-1}. It has been shown in the present study that the corrosion behavior of PD CASTA H and PD 2000 alloys, containing Co and a high Cr content, displays the best corrosion resistance compared to CERACAST NB alloy. The influence in the temperature and pH of the solution had effects on the properties of dental alloys. The electrochemical behavior of dental alloys were studied to provide a comprehensive examination of various biomedical materials used in dental application. However, the surface roughness and the surface morphology of the alloys are very important in dental study and application.

KEYWORDS

Artificial saliva

Atomic force microscopy

Biocompatibility

Chromium-cobalt alloys

Corrosion

Cyclic voltammetry

Dental alloys

Electrochemical mesurement

Microstructure

Nickel-chromium alloys

Organic acids

pH

Potentiodynamic polarization

Resistance

Scanning electron microscopy

Secondary ion mass spectrometry

Temperature

X-ray diffraction

ACKNOWLEDGEMENTS

First and foremost, I thank God (Allah) for giving me the ability and good health to complete this study and the thesis writing successfully.

- My gratitude is extended to my supervisor, Professor Dherendra Gihwala for his continuous supervision, support, commitment, and for providing me with the opportunity to study at Cape Peninsula University of Technology (CPUT).
- My co-supervisor, Professor Malik Maaza from iThemba LABS, for his excellent supervision, encouragement, patience and motivation throughout the study.
- Dr. Johan André Mars at Cape Peninsula University of Technology (CPUT), for his assistance and advice, most of all his inspiration.

I would also like to give a heartfelt thanks to my co-mentor Dr Ntevheleni Thovhogi from iThemba LABS, for her valuable advice, guidance and encouragement during this study. Her assistance throughout the experiments and writing of the thesis is really appreciated.
My sincere gratitude also goes to the late, Professor Abel Jacobus Esterhuyse, the head of the Department in the Biomedical Sciences, Faculty of Health and Wellness Sciences, Cape Peninsula University of Technology, who passed away a few months ago, who was always guiding, motivating and encouraging me during the study. May his soul rest in peace.
I would also like to use this opportunity to express my gratitude to people from iThemba LABS:

- Dr. Chester Kotsedi, for his advice and helping with anything I needed for this study.
- Mr. Zakhele Khumalo, for assisting in the XRD measurements.
- Dr. M. Nkosi, for AFM imaging and results analysis.
- Dr. Zebib Yenus, who was always willing to assist when I required her help.
- Miss Xanthene Muller, at Radioiology LABS, for her assistance in using the equipments.
- Dr. Bertrand Tumbain Sone, who was always willing to assist when I required his help and for his invaluable support and assistance in SIMS measurement and analysis.
- Mr. Adrian Josephs at the University of Western Cape, for helping me with SEM–EDS measurements.
- Dr Abd Almonam Baleg at the University of Western Cape, for his advice and assistance with electrochemical measurements.

- The staff of the National nano surface characterization facility, at the Physics Department, University of the Free State, Bloemfontein, South Africa, for their assistance with SIMS measurement and analysis.

Furthermore, I wish to thank:

My mother, Fatima, who has always prayed for me, for her unconditional love and for her hard work and persistence, which has served as an invaluable example to me.

My husband Osama, who encouraged me to do my best in everything that I have undertaken.

My sons Gehad & Mohammad who always gave me a smile under the worst conditions.

The deepest appreciation goes to my brothers and sisters for their motivation and constant encouragement.

My country Libya for offering the funding and opportunity to study abroad and all the staff at Libyan embassy in Pretoria, South Africa, for their continued support and financial assistance throughout this study.

The Faculty of Medical Technology and Dental Technology Department in Misurate, Libya, for the opportunity given to me.

Everyone who has made a contribution towards the completion of this research project.

DEDICATION

To my late father (Nuoh), and my brother (Mohammad)

Who were always in my heart.

Had they been alive, they would have been be so proud of my success. You meant so much to me.

ABBREVIATIONS

ADA	American Dental Association
AE	Auxiliary electrode
AFM	Atomic force microscopy
Co–Cr	Cobalt-chromium
*cp*Ti	Commercially pure titanium
CV	Cyclic voltammetry
E_{corr}	Corrosion potential
EDS	Energy dispersive spectrometry
EIS	Electrochemical impedance spectroscopy
E_{pa}	Anodic peak potential
E_{pc}	Cathodic peak potential
FPD	Fixed partial dentures
i_0	Corrosion current density
i_{pa}	Anodic peak current
i_{pc}	Cathodic peak current
MIC	Microbially-influenced corrosion
Ni–Cr	Nickel-chromium
OCP	Open circuit potential
OCP	Open circuit potential
PFM	Porcelain-fused-to-metal
pH	Power of Hydrogen
R_a	Mean roughness
R_E	Working electrode
RMS	Root mean square
R_p	Polarization resistance
SEM	Scanning electron microscopy
SIMS	Secondary ion mass spectrometry
TOF–SIMS	Time of flight secondary ion mass spectrometry (TOF-SIMS)
WE	Reference electrode
XRD	X-ray Diffraction

Contents

List of Figures

List of Tables

CHAPTER 1

Introduction

1.1 Clinical viewpoints

1.1.1 Dental anatomy

The structure of tooth is a complex composite of soft and mineralized tissues. The oral environment is the first area in which digestion of the food begins. It is therefore necessary to maintain the total health of the mouth and thus maintain a healthy immune system. Not only do the teeth serve multiple functions in the chewing process, but also have an effect on the æsthetic appearance and speech of the person.

1.1.2 Tooth development

A human being has two sets of teeth in their lives, the primary teeth, also called the milk or baby teeth and the permanent teeth referred to as the secondary or adult teeth. An infant has 20 primary teeth, which are replaced by the 32 permanent at the age 13. There are four types in both arches. These are the incisors, the canines, the premolars and the molars. Each one has a different function and is located in a different area of the mouth. The tooth with two major parts in their structure, the crown and the root (Awan, 2010) is shown in figure 1.1. The cross section of any tooth consists of four major tissues the enamel, the dentin, the cementum and the pulp. All these parts play important roles in the functioning of the teeth. The teeth are divided into sections and named according to their function with each tooth having a root and crown portion. The crown is covered with enamel and the root is embedded into the alveolar processes and is covered with cementum (Van Noort, 2002). The crown is the visible part of the tooth, above the gum line and is covered with an enamel coat, comprising the crown. Enamel is the hardest substance in the human body and is composed of 95%[1] minerals, mostly hydroxyapatite, $Ca_{10}(PO_4)_6)F_2$. Enamel is incapable of being remodelled or repaired (Brand & Isselhard, 2003). The cementum covers the root of the tooth while dentine constitutes the matrix of the tooth. Although it is tissue, it is harder than bone. It is also porous due to its tubular structure and often becomes sensitive to stimuli, such as, temperature variations, air and

[1] For the purpose of this study, the concentration denoted by % implies the parts of mass of substance per 100 parts of the matrix

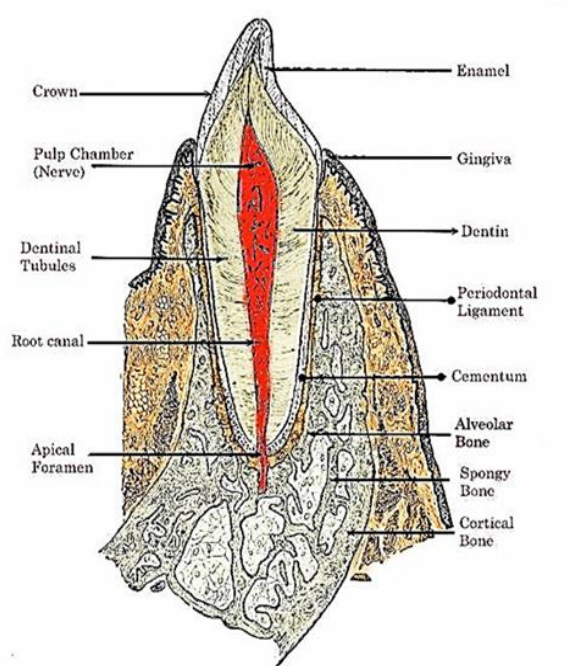

Figure 1.1: Illustration of the tooth anatomy, showing the crown, root sections and various other parts of the tooth anatomical structure (Awan, 2010).

touch (Brand & Isselhard, 2003).

During early development, the dentine and pulp are closely related in the function and structure, and at maturity, the structures are different. Together, the dentine–pulp complex shows a range of responses to caries of the dental tissues, which represents a summation of injury, defense and repair mechanisms (Smith, 2002).

1.1.3 Origin of dental caries

Dental caries is one of the most prevalent chronic dental diseases in the world. It results from dental erosion due to bacterial acids derived from the microbial plaque which consequently cause cavities (Ardakani *et al.*, 2004). Dental caries arise from the surface demineralization of the tooth, that is caused by acids which are produced by acidogenic bacteria present in the surface plaque (Massler, 1967). There are several bacterial strains in normal flora of oral cavity. The dental plaque is formed from a mixture of food, saliva and other organic compounds inside oral cavity (Lawrence & Marshall, 1999). Bacteria are found mainly inside the dental plaque and dental calculus and on the surface of soft tissue (Lawrence & Marshall, 1999). *Streptococcus mutans* (*S. mutans*) is one of the bacterial microorganism that grows in dental plaque, and is the predominant dental–caries causing bacterium. Other bacteria that have also been implicated, include *S. sobrinus, Actinomyces sp*, and *Lactobacillus sp*.

The accumulation of acid produced by *S. mutans*, results in lowering of the pH level in saliva, and causes demineralization of the enamel (Hung, 2008). Enamel mainly consists of calcium phosphate, $Ca_3(PO_4)_2$, in the form of a pyramidal crystal structure, which is demineralized when the pH level of the

environment is lowered by the organic acid resulting in the pyramid structure begin destroyed leading to dental caries. The bacteria will continue to produce acid and then destroy the dentin and further penetrate the dental pulp leading to pulpal infection and this will lead to a dangerous level of infection transmitted to other organs in the body through the circulatory system of the dental pulp (Hung, 2008). The cycle of

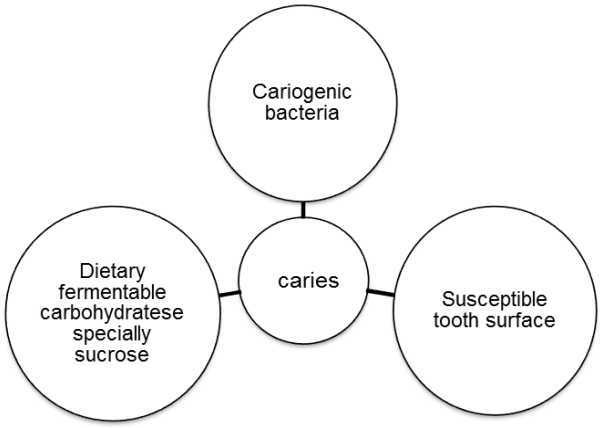

Figure 1.2: Illustration of dental caries as a multi–factorial disease (Peterson, 2001).

dental caries is presented by three overlapping circles as a model of the stage factors needed for dental caries formation, as shown in figure 1.2. The circles showed the elements: bacteria, diet, and teeth, all of which are present for dental caries to form. There are another risks causing dental caries including oral flora, feeding and eating practices, tooth anatomy and enamel defects, deep pits fissures, saliva, and pH levels.

1.2 Alloys

Many different alloys are used as dental materials for fixed and removable partial dentures, filling, orthodontic devices and implants. Alloys used in oral environments are exposed to different conditions, which may lead to chemical degradation such as corrosion.

The materials employed in the mouth should be completely tarnish– and corrosion–resistant. It must neither react with the many alkaline and acid foods that are taken into the mouth, nor must it be affected by mouth fluids. Furthermore, it must be extremely strong so that the tooth restorations and appliances will not be broken or bent by the forces exerted during chewing (Philips & Skinner, 1965). Human saliva is composed of a mixture of organic and inorganic ingredients. This plays an important role in the choice of restorative materials (Jenkins, 1985). Insufficient corrosion resistance leads to discoloration and deterioration of the mechanical properties while the corrosion products can harm the biological system of the host (Bergman *et al.*, 1980).

Corrosion of dental alloys has biological, functional as well as æsthetical effects and the use of non-precious alloys in crown-and-bridge restorations is a much discussed subject, notably because the release of metallic components and ions from a prosthetic restoration could be harmful to the health

status of a patient. Corrosion may be described as the deterioration of materials by aggressive action of the environment. As such as the oral environment is very conducive to corrosion. Fluctuations in temperature, the presence of moisture, change in pH because of diet, variations in oxygen pressure, and decomposition of food all contribute to this process (Gill *et al.*, 1999). The most important alloys in this respect are nickel-containing alloys which are still used widely in dental restorations but are suspected to cause allergic reactions (Finne *et al.*, 1982).

Electrochemical corrosion occurs particularly when two or more different alloys are present in the oral cavity (Raghavan, 1981). Metal ions which are released from dental alloys in the humid oral cavity medium can lead to either toxic or allergic responses. They can be transferred to distant organs, thereby causing different changes (Bergman *et al*., 1980). Base metal alloys exhibit a greater number of released ions than the alloys containing larger amounts of gold (Johansson *et al.*, 1989a).

1.3 Biocompatibility of dental casting alloys

There are four groups of materials used in dentistry. These are metals, ceramics, polymers and composites. Dentists and materials scientists will continue the search in the 21^{st} century for the ideal restorative material. An ideal restorative material would (1) be biocompatibility; (2) bond permanently to the tooth structure or bone; (3) Match the natural appearance of tooth structure and other visible tissues; (4) Exhibit properties similar to those of tooth enamel, dentin, and other tissues, and (5) Be capable of initiating tissue repair or regeneration of missing or damaged tissues (Anusavice, 2003a).

Dental materials should also withstand the effects of most severe environment. Variations in temperature and acidity or alkalinity and high stresses all have an effect on the properties of materials. Normal temperature variations in the oral cavity ranges between 32^0C and 37^0C. However the acidity or alkalinity of fluids measured in the oral cavity by pH varies from around 4 to 8.5, while the intakes of acid fruit juices or alkaline medicaments can extend this range from pH 2 to 11. The dental materials selected for use as replacements for natural tissues place a very high demand upon the chemical, physical and biological properties. According to McCabe & Walls (1998) dental materials must be:

- Compatible with biological tissues and without eliciting any adverse reactions,
- Capable of responding successfully to the stresses and strains,
- Capable of withstanding the corrosive environment,
- Capable of simulating in most cases the appearance of natural tissues, in terms of both colour and translucency, and
- Capable of being reasonably easy to fabricate by traditional methods.

The human body is not an environment that one would consider hospitable for an implanted metal alloy. It has a highly oxygenated saline electrolyte at a pH of around 7.4 and a temperature of 37^0C. While it is well known that chloride solutions are among the most aggressive and corrosive to metals, the ionic composition and protein concentration in body fluids complicate the nascent understanding of biomedical corrosion even further. Variations in alloy compositions can lead to subtle difference in mechanical, physical or electrochemical properties. However, these differences are minor compared with the potential variability caused by differences in fabrication methodology (Douglas, 2008).

When any prosthetic appliance is inserted into the oral cavity, the dental alloy will be contact with saliva. Saliva is a hypotonic solution consisting of approximately 99% water, containing a variety of electrolytes (sodium, potassium, calcium, chloride, magnesium, bicarbonate, phosphate) and proteins, represented by enzymes, immunoglobulin and other antimicrobial factors, mucosal glycoproteins, traces of albumin and some polypeptides and oligopeptides of importance to oral health (De Almeida *et al.*, 2008).

The presence of fluoride in saliva, even at physiologically low levels, is decisive for the stability of dental minerals. Its concentration in total saliva is related to its consumption. It is dependent on the fluoride in the environment, especially in drinking water. Other sources are also important, such as dentifrices and other products used in caries prevention. The presence of fluoride ions in the liquid phase reduces mineral loss during a drop in biofilm pH, as these ions diminish the solubility of dental hydroxyapatite, making it more resistant to demineralization. It has also been demonstrated that fluoride reduces the production of acids in biofilm (De Almeida *et al.*, 2008). Normal salivary pH is from 6 to 7 and varies in accordance with the salivary flow, from 5.3 (low flow) to 7.8 (peak flow). There are various sources of hydrogen ions in oral fluids: These include the secretion by the salivary glands in the form of organic and inorganic acids or ions. These ions influence the equilibrium of calcium phosphates in the enamel (De Almeida *et al.,* 2008). The higher the concentration of hydrogen ions, the lower the pH and vice versa (Humphrey & Wiliamson, 2001; Tenovuo *et al.,* 1994). At higher flows of stimulated salivary secretion, the concentration of bicarbonate ions is higher, the pH also rises and the buffering power of the saliva increases dramatically (Axelsson, 2000).

Many orthodontic appliances are also fabricated from metallic materials. It has been documented *in vitro* and *in vivo* that metallic dental devices release metal ions, mainly due to corrosion (Geurtsen, 2002). Casting alloys and commercially pure titanium are widely used in modern dentistry for temporary and permanent restorations, splints, and removable or fixed orthodontic appliances. It has been hypothesized that the severity of physiological effects of the alloy significantly depends upon the type of metal, its chemical state and concentration (Schmalz *et al.,* 1997; Yamamoto *et al.*, 1998). Those metallic components may be locally and systemically distributed and could play a role in the ætiology of oral and systemic pathological conditions. The quality and quantity of the released cations depend upon the type of alloy and various corrosion parameters. No general correlation has been observed between alloy

Table 1.1: Quantitative elemental composition of precious and non-precious alloys (Craig, 1997).

Precious alloys	Non-precious alloys
Nobel metal content > 60% Gold (Au) content > 40%	Noble metal content < 25% Base metal content > 25%
Noble metals	Base metals
Gold (Au), platinum (Pt), palladium (Pd), iridium (Ir), ruthenium (Ru), rhodium (Rh)	Silver (Ag), copper (Cu), zinc (Zn), indium (In), tin (Sn), gallium (Ga), chromium (Cr), cobalt (Co), molybdenum (Mo), aluminium (Al), iron (Fe), beryllium (Be), manganese (Mn), titanium (Ti), nickel (Ni), vanadium (V),niobium (Nb), zirconium (Zr).

nobility and corrosion (Geurtsen, 2002). The American Dental Association (ADA) Specifications classify alloys into three groups as showed in table 1.1. It should be emphasized that silver is a noble element in metallurgy but based upon its relatively high reactivity in the oral cavity, silver is considered by the ADA to be a base metal (Anusavice, 1996).

Due to the significant increase in the price of gold over the past 20 years, the use of both gold-reduced noble alloys and base metal alloys has significantly. Castable *cp*–Ti has also received increasing interest and importance for fabrication of fixed and removable restorations (Berstein *et al.*, 1992; Geurtsen, 1994).

1.4 Dental alloy classification

Dental alloys are widely used as constructive materials in the fabrication of dental restorations. Dental alloys are multi-component alloys which consist of solid solutions of metals and non-metals. With the process of alloying, the required properties of metal can be improved and harmful ones diminished. An alloy is composed of basic metal and alloying elements, which can be either metals or non-metals (Knosp *et al.*, 2003). Among numerous dental alloys, those which are of a special significance are alloys classified as "precious" (Knosp *et al.*, 2003).

Precious dental alloys are in the form crystalline materials. Atoms of elements which form a crystal lattice, are periodically arranged spatially in a regular fashion. Such an order extends throughout the areas, which are very large compared with the inter-atomic distances. The arrangement of atoms in a crystal lattice gives an ideal crystal structure according to the principles of geometric crystallography which is the most stable structure in all technical materials from the thermodynamic viewpoint. In special conditions precious dental alloys may harden into an amorphous material but only if the transition from the melted into a hardened state is fast enough so that atoms cannot be arranged in the thermodynamically most stable position (amorphous metals). This is usually achieved in dental technology laboratories under controlled speeds hardening and cooling. Normally real crystal structure, as shown in figure 1.3, is achieved which may deviate from an ideal structure (Stamenkovic *et al.,* 2009).

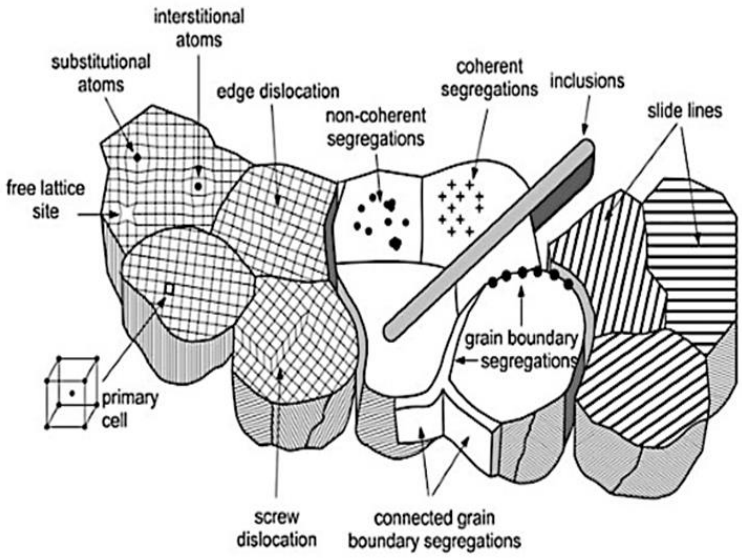

Figure 1.3: Possible defects in a dental alloy basic structure caused by repeated melting and casting (Stamenkovic *et al.*, 2009).

1.5 Gold alloys

Historically, Gold is the oldest dental restorative material, and has been used in dentistry for more than 4,000 years due to its good biocompatibility and versatility (Knosp *et al.,* 2003; Fischer, 2002). Over the past 20 years the price of gold has risen significantly in the world market. The high price of gold led to a wider use in dental prosthetics of the precious alloys with a lower gold content, as well as the basic alloys. On the other hand, once melted and cast, precious dental alloys are being re–melted and re–casted. It is often impossible to determine the number of melting and castings because the weight of new alloys that are added cannot be determined (Stamenkovic *et al.*, 2009). Gold alloys are principally used for all–metal restorations (inlays, crowns and onlays) in single posterior teeth. These alloys are cast by a precision investment process and the restorations are cemented by the dentist into the prepared tooth cavity (William & Satish, 2012).

The original gold casting alloys contained over approximately 70% gold, but the high price of gold has led to the development of alloys that contain approximately 50% gold. These alloys also contain silver, copper, platinum, palladium, zinc, and minor components as well as other trace elements, including iridium for grain refinement (Anusavice, 2003b; Powers & Sakaguchi, 2006). In conservative and restorative dentistry, as well as in orthodontics, gold is used either as a pure metal, or alloyed together with noble metals and base metals. This use of pure gold is limited to direct filling of small occlusal cavities and no standard exists for the application and properties of direct filling gold. However, with an increasingly wide range of alternative materials available for dental repairs, it is considered appropriate to review the current gold based technology available today and thereby highlight the exceptional performance that competing materials must demonstrate if is to displace gold from current uses (Knosp *et al.*, 2003). Inlays, onlays and partial crowns from high gold alloys can be precisely fabricated in the dental laboratory with

an excellent marginal fit and longevity of many years. Full cast or partially veneered crowns are mostly used for posterior teeth because gold (as well as other metallic materials) should not be visible in the anterior area (Knosp *et al*., 2003). An example of a gold crown is shown in figure 1.4.

Figure 1.4: An example of a crown made from gold–containing alloy.

1.6 Gold crown made from gold alloys

1.6.1 Alloys for fixed prosthodontics (metal-ceramic restorations)

Ceramic structures are used to replace missing teeth. Tooth structure lost to disease or trauma and for aesthetic reasons. Recreating aesthetics and functionality are the two practical goals of such restorative treatment. Aesthetics is an obvious attribute of ceramics and along with durability, is the primary reason dentists often choose ceramics over other materials. Functioning includes chewing, speech, and the maintenance of a healthy harmony among teeth. Supporting bone and soft tissues and the muscles of mastication (Kelly, 1997).

Metal–ceramic restorations are in widespread clinical use for restorative and prosthetic dentistry and are employed for single-tooth restorations and for restorations involving multiple adjacent teeth (fixed prostheses or crown-and-bridgework) (William & Satish, 2012). Metal–ceramic prostheses have been used in dentistry for many decades and have a record of good clinical performance, aesthetic and durability (Anusavic, 2006; McCabe & Walls, 2008). It is composed of a metallic framework and a ceramic veneer. The former is regarded for the mechanical resistance and the latter for the aesthetic part of the prostheses (Henriques *et al.,* 2012). An alloy is cast using the precision investment procedure in dental laboratories to fit accurately to the prepared tooth or teeth and to form a substrate (termed the coping) for the porcelain. After an initial oxidation step that forms a native oxide on the metal surface, one or two layers of opaque porcelain are bonded to the metal, followed by the application of a layer of body

porcelain and a surface glaze (Anusavice, 2003b; Powers & Sakaguchi, 2006). In order to have a strong bond between the porcelain and metal, which is essential for clinical longevity of the metal-ceramic restoration, the coefficients of thermal contraction for the metal and porcelain must be closely matched, and a difference not exceeding 0.5 ppm^0C^{-1} is generally desired (William & Satish, 2012). In the substructure design, ceramics are simply substituted for cast metals in ways that mimic its use. Most clinicians and manufacturers have assumed that metal-ceramic prostheses were structurally successful simply because of the support given by the casting to aesthetic dental porcelains. Framework design principals taught in dental texts invariably include the need for proper support of porcelain (Rosentiel *et al.*, 1995; McLean, 1980).

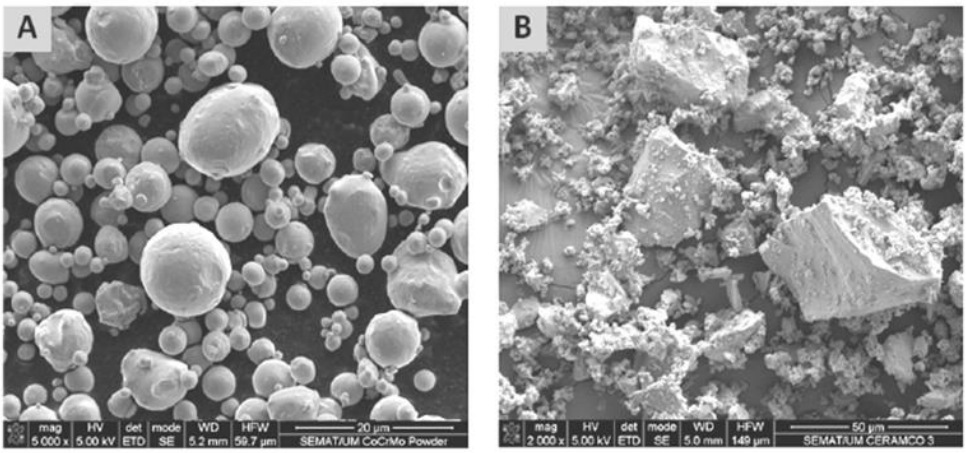

Figure 1.5: Electron micrographs of (A) a Co–Cr–Mo dental alloy (Nobil4000, Nobilmetal, Villafranca dAsti, Italy) in powder form. The alloy powder particles have spherical shape (Henriques *et al.*, 2012) and (B) of an opaque porcelain powder (Ceramco3, Dentsply, New York, USA) (batch number: 08004925) (Henriques *et al.*, 2012)

1.6.2 Alloys for removable prosthodontics

Since the price of gold rose significantly in the 1930s, a large number of new non-noble alloys were developed for use in dentistry apart from the Au–Pt alloys. The Au–Pt alloy is a high noble alloy, while the Co–Cr–Mo, see figure 1.5, alloy used for fabrication of casting alloy (metal framework) dentures or the Ni–Cr alloys used for dental metal ceramic appliances are base–metals or non–noble alloys (Craig *et al.*, 1983). Base metal casting alloys (nickel–chromium, cobalt–chromium and cobalt–chromium–nickel) are popular for fabricating the metallic frameworks for removable partial dentures because of their lower cost (Anusavice, 2003; Powers *et al.*, 2006). Nickel-chrome casting alloys were developed as an alternate, because of their superior properties in relation to porcelain-fused-to-metal (PFM) applications, high strength for crowns and fixed partial denture, better elongation percentage and high elastic modulus for removable partial denture (Bumgardner & Lucas, 1993). Nickel is considered to be the most common

allergen in dental alloys (NIDR, 1984; Morris *et al.*, 1991).

Chromium and nickel impart corrosion resistance and mechanical strength to non-precious alloys. It has been observed that in nickel alloys with a chromium content of over 20% and a molybdenum content of greater than 4% can ensure adequate corrosion resistance (Johansson *et al*.,1989a; Huang, 2002a). The presence of Cr improves the corrosion resistance of alloys in a corrosive environment due to the formation of a Cr–rich, passive oxide film which is highly resistant to acid (Sharma *et al*., 2008). Molybdenum in the Ni–Cr based alloy increases the resistance to localized corrosion in the chloride containing environment (Schiff *et al.*, 2002). Therefore, for base–alloy dental materials, the addition of 12% Cr (minimum value) and 2–5% Mo to the alloy bulk is recommended from the corrosion resistance point of view (Anusavice, 1996).

There is much literature on corrosion studies of dental alloys in natural or artificial saliva media. However only a few studies of dental materials in saline solutions to emulate aggressive corrosion conditions in the oral cavity have been reported (Sharma *et al*., 2008). In one study Sun *et al*. (2002) have used 0.9% and 0.09% NaCl solutions in simulated environments for corrosion studies of various non-precious and noble dental alloys using open circuit potential (OCP) and cyclic polarization measurements was made. Lucas *et al.* (1991) have used 0.9% NaCl medium as an *in vitro* medium for studying Co–Cr and Ni–Cr alloys using electrochemical techniques. Dong *et al* (2003) examined corrosion resistance behaviour of Co–Cr and Ti using immersion tests in various types of electrolyzed water. Johanson *et al.* (1989b) have studied corrosion of copper–nickel alloys in saline solutions using electrochemical techniques. Geis–Gerstorfer *et al.* (1991) analysed corrosion of various Ni-–Cr—Mo and Co—Cr—Mo alloys in 0.1 M NaCl solution by weight loss over a 5 week duration. Huang (2002b) has used 1% NaCl in the halide solutions for the study of corrosion resistance of chemically pure titanium (*cp*Ti).

1.6.3 Titanium alloys

Titanium is considered to have a high biological affinity and it has been intensively applied in the manufacturing of biomedical devices since the 1980s (Cremasco *et al.,* 2008). Titanium and titanium alloys are used on the biomedical applications for their low density, excellent biocompatibility, corrosion resistance and mechanical properties. Also been used in dental implants. Since the oral environment could involve a fluoride medium, the degree of corrosion resistance offered by the Ti alloys in a fluoride–containing medium becomes an important criterion in the selection of a metallic biomaterial to be used in the oral medium (Kumar & Narayanan, 2008). The elements that cause the corrosion of titanium in oral environments are many, but in general, microbially–influenced corrosion (MIC) is deemed to be the main reason. The mechanisms involved in oral environments are very complicated, as the process is affected by many factors (Qing *et al.,* 2014). One of the main metabolic substances in oral environments lactic acid, exists naturally in the human oral cavity as a product of the oral cell tissues and of the bacteria (Grimsdottir & Hensten–Pettersen, 1993). The role of lactic acid in the corrosion of titanium is an important to further

explore the effect of MIC in oral environments. There are many studies that showed the effect of lactic acid on titanium in oral environments.

Mabilleau *et al.* (2006) investigated the corrosion resistance of CP-Ti disks for nine days of immersion in different test solutions based on artificial saliva containing F–H_2O_2, and lactic acid by AFM and SEM. Their results showed that the surface roughness was highly increased when titanium disks were immersed in artificial saliva containing F–H_2O_2 and lactic acid. Koike *et al.* (1997) and Koike & Fujii, (2001) reported that titanium has a high resistance to corrosion in physiological saline and artificial saliva by immersion tests. It was dissolved and became discoloured when in contact with lactic acid or formic acid. Masatoshi *et al.* (2011) evaluated the corrosion resistance of Ti–Ag alloys in a 1% lactic acid solution. It showed that the Ti–Ag alloys had excellent corrosion resistance that was comparable or superior to that of pure titanium.

Corrosive properties of titanium were markedly dependent on pH in formic acid and relatively less dependent on pH in lactic acid. However, up to now, there have been few reports studying the effect of lactic acid and the mechanism remains unclear (Qing *et al*., 2014).

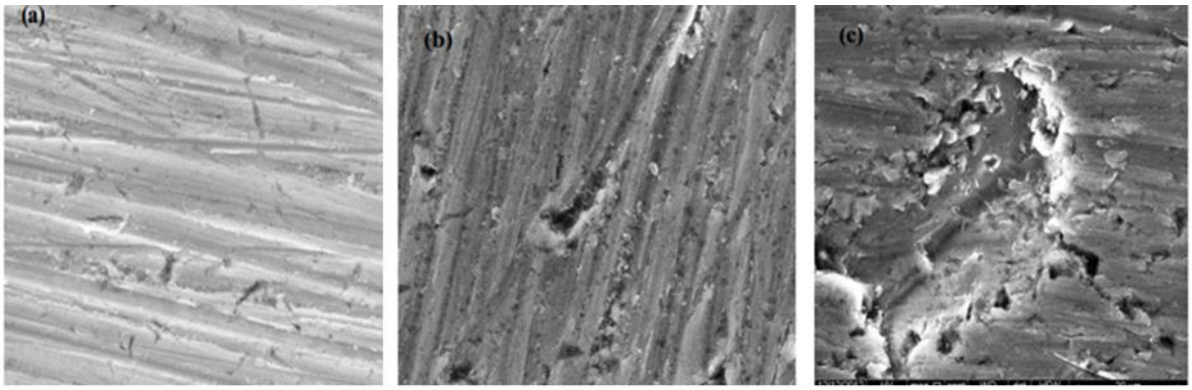

Figure 1.6: Surface morphologies of titanium immersed in artificial saliva: (a) in the absence of lactic acid, (b) in the presence of 3.2 g/L, and (c) 5.0 g/L lactic acid (Qing *et al.,* 2014)

In figure 1.6 are show the surface morphologies of titanium immersed in artificial saliva in the absence of lactic acid and in the presence of 3.2 and 5.0 g/L lactic acid two weeks. The surface, in the absence of lactic acid, looks rather smoother, that is, the corrosion attack in the absence of lactic acid is more uniform in character and there is little tendency towards local enrichment of products on the surface (Qing *et al.*, 2014). By comparison, figure 1.6c shows bigger and deeper pitting than those in figure 1.6b. The addition of lactic acid therefore can significantly affect the formation of pitting. Consequently, at the microscopic level, the effect of lactic acid on generating pitting cannot be ignored. Additionally, the adsorption of lactic acid in the micro-point of pitting corrosion can hinder titanium passivation, providing a necessary premise and driving force for generating macro-pitting corrosion (Qing *et al.*, 2014).

1.6.4 Corrosion mechanisms

1.6.4.1 Chrome (Cr)

In the presence of air, chromium metal spontaneously forms a layer of passive oxide layer of Cr_2O_3. The formation of Cr_2O_3 at the electrode surface and its further oxidation to CrO_4^{2-} at higher potentials leading to the recorded anodic peak, can be represented by the reactions given in table 1.2 (Kovacevic *et al*, 2012).

Table 1.2: Reduction and oxidation of chromium (Cr) species.

Reaction
$Cr\,(s) + H_2O(l) \rightleftharpoons Cr_2O_3(s) + 6H^+(aq) + 6e^-$
$Cr_2O_3(s) + 5H_2O(l) \rightleftharpoons 2CrO_4^{2-}(aq) + 10H^+(aq) + 6e^-$
$CrO_4^{2-}(aq) + 14H^+(aq) + 6e^- \rightleftharpoons 2Cr^{3-}(aq) + 7H_2O(l)$
$Cr(s) + 3\,e^- \rightleftharpoons Cr^{3-}(aq)$

1.6.4.2 Nickel (Ni)

In the presence of air, nickel metal spontaneously forms a layer of passive oxide layer of NiO. The formation of NiO at the electrode surface and its further oxidation to species such as Ni_2O_3 at higher potentials leading to the recorded anodic peak, can be represented by the reactions given in table 1.3 (Kovacevic *et al*, 2012).

Table 1.3: Reduction and oxidation of nickel (Ni) species.

Reaction
$Ni + H_2O \rightleftharpoons NiO + 2H^+ + 2e^-$
$3NiO + H_2O \rightleftharpoons Ni_3O_4 + 2H^+ + 2e^-$
$2NiO + H_2O \rightleftharpoons Ni_2O_3 + 2H^+ + 2e^-$
$Ni_2O_3 + H_2O \rightleftharpoons 2NiO_2 + 2H^+ + 2e^-$
$Ni^{2+} + 2e^- \rightleftharpoons Ni$

1.7 Problem statement

Dental alloys have been widely used in contact with oral tissue. The most important property of an alloy is its corrosion resistance and concomitantly, its biocompatibility (Wataha, 2000).

Nickel–chromium (Ni–Cr) alloys are used in crown and bridge casting, and also in orthop ædic implants like plates, pins and screw. However, accounting for unique conditions related to biological considerations, there are other factors that will affect the choice of alloys which has acceptability. This can prove useful in addressing some problems related to the biocompatibility of the biomaterial. The advantages of these alloys include low cost of casting, matching the thermal expansion coefficient with the ceramics of metal-ceramic restorations, and acceptable mechanical and *in vivo* tribological properties

(Schmalz & Garhammer, 2002). Metal restorations have been among the most popular restorations used in the fixed partial dentures (FPD) for the last four decades. Successes of these systems are related to its long–lasting durability and acceptable æsthetic properties. However, the metal substructure of these systems can lead to toxicity and allergic reactions in some patients because of the corrosion that can occur in the metal. This corrosion can also lead to pigmentation of the gingiva (Freilich & Meiers, 2004). However, many dental casting alloys which have good mechanical properties, on the one hand, are not good enough from the aspect of corrosion because of their complex structure (Russell & Yiming, 1998). Organic acids, which are created after disintegration of food remains decrease the pH value inside the oral cavity and may have an effect on the ion–release from dental alloys. This can have a negative effect that can lead to either toxic or allergic responses. Also, the materials used in the mouth must resist the humidity and the changes in temperature inside the mouth, which happens during the chewing process inside the oral cavity (Philips, 1991).

1.8 Background to the problem statement

Dental alloys are widely used in dentistry, especially in contact with oral tissues. It is of paramount importance to understand and get familiar with biocompatibility of alloys for their long term success in rendering successful treatment for the patients. One of the most relevant properties of a casting alloy to its biological safety is its corrosion resistance (Wataha, 2000). A biomaterial is used to restore or replace the function to a body tissue and is continuously in contact with body fluids (Agrawal, 1998). The three main classes of biomaterials include metals, polymers and ceramics. Along with these, biomaterials are also composed of certain natural materials like collagen which also play a significant role in the multidisciplinary field of tissue engineering (Langer, 1999; Castner & Ratner, 2002). The choice of an alloy is based on several factors.

- Cost is a serious consideration due to the high price of gold. These factors in particular limit the use of alloys for dental prostheses;
- The choice of a specific application is primarily determined by their mechanical properties, such as hardness, mechanical strength and ductility (Van Noort, 1994) and
- The choice of specific prosthetic laboratory, experienced in the manufacture of the material and of the experience of the dental practitioner is also important for the casting quality.

In 1972 the American Dental Association (ADA, 1972) proposed a program for acceptance of metal alloys, aiming at evaluating all metal alloys for cast restorations, including those not included in its specifications. Also considered was all alternative alloys to the gold-based alloys and those which were a part from their composition, demonstrated biological compatibility and adequate physical, chemical and mechanical properties (Karina *et al.*, 2004).

Noble metal alloys have successful clinical use but because the price of gold increased, alternative cheaper based alloys (Ni–Cr, Co–Cr) were developed (Wang & Yiming, 1998). Alloys such as (Ni–Cr, Co–Cr) have been used in the fabrication of removable and fixed partial dentures for their excellent mechanical properties and corrosion resistance character. In dentistry, the most important factors affecting the choice of dental alloys are biocompatibility, mechanical properties and resistance to tarnish and corrosion (Lawson, 1991). When selecting a dental casting alloy for clinical application, the decision will depend on the physical properties of the alloys, biocompatibility, and good mechanical properties, such as hardness, strength, resistance to tarnish and high temperature and also resistance to corrosion. The humid, warm oral cavity offers ideal conditions for corrosion of the metal surface to take place and dissolving of the teeth subsequent. Foods and drinks are usually very acidic or alkaline. Different organic acid, such as lactic and pyruvic acid are created after disintegration of some food (Philips & Skinner, 1965). Organic acids decrease pH value inside the oral cavity and may have a negative effect on ions releases from dental alloys. Metal ions which are released from dental alloys in the oral cavity can lead to either toxic or allergic responses (Morris, 1987).

Furthermore, they can be transferred to other organs, thereby causing further changes to the organs. As mentioned earlier, as the price of gold increase, new dental alloys appeared on the market. Some of these new alloys released much more ions than conventional alloys (Johansson *et al.*, 1989a). Studies on these new materials also showed that ions released from different dental alloys were not directly proportional to ion concentration in the alloys but due to the fact that some elements in the alloys are more unstable than others. This phenomenon is referred to as “selective dissolving” (Wataha *et al.*, 1991). In general, corrosion rates of metal and alloys can be determined using chemical and electrochemical methods. Chemical methods used for finding the corrosion tendency of alloys, can be done by determining the mass loss of corroding metal and alloy, the amount of corrosion products in the corrosive media or the amount of gas produced during the corrosion reaction (Mansfeld, 1976).

1.9 Aim and objectives

The aim of this study was to evaluate the influence of temperature and pH on corrosion resistance of Ni–Cr and Co–Cr dental alloys. The objectives of this work were:

- To characterize the physical and mechanical properties of Ni–Cr and Co–Cr alloys on corrosion resistance after being immersed on artificial saliva; and
- To investigate the correlations between corrosion and biocompatibility of dental alloys and to interpret the results by comparison with ion concentrations found in food.

1.10 Research hypothesis

Three alloys, namely, PD CASTA H (Cr–Co), CERACAST NB (Ni–Cr) and PD 2000 were investigated in this study. These alloys will for the purpose of the hypothesis will be referred to as $S_i; i = 1, 2, 3$. The alloys were subjected to two experimental conditions at 1) two pH values of 2.5 and 6.5, denoted by $p_i; i = 1, 2$ and at 2) three temperatures, 25^0C, 37^0C and 40^0C, denoted by $T_i; i = 1, 2, 3$. The principal aim of this study is to assert that anyone of the alloys will not corrode when subjected to both the experimental conditions. The null hypothesis, H_0, indicates that 'no effect' or 'no difference', that is, when each of the alloys are subjected to the experimental conditions then all three alloy will corrode; expressed logically: $H_0 : \forall(p_i \wedge T_i)S_i = 0$. The alternative hypothesis, H_a, is that when any of the three alloys is subjected to the experimental conditions, then anyone one of the alloys will not corrode; expressed logically: $H_a : \forall(p_i \wedge T_i)S_1 \vee S_2 \vee S_3 = 1$.

1.11 Overview of thesis

Chapter One: This chapter focused on the literature review of dental materials, and the biocompatibility properties in the oral cavity with reference to relevant previous studies that are closely aligned to this study. The background of using dental materials and alloys, the aims and the objectives of the research also discussed in this chapter.

Chapter Two: This chapter entails the analytical techniques used to confirm or disporove the aims of the study. A brief discussion of the chemistry and physics–based principles of the techniques is given. This was necessary as these fundamentals do not include or explicitly stipulates the applicability of the techniques to the specimens. Additional aspects were incorporated into the fundamental equations underlying these analytical techniqes, hence might support the findings in this study.

Chapter Three: This chapter presents the instrumentation used to perform the analysis, general methodology, that is, the adaptation of instrumental paramenters to achieve optimum results for this study.

Chapter Four: This chapter entails the presentation and discussion of the results obtained from each analytical technique and how these separate results were combined to achieve the aims of the study.

Chapter Five: This chapter highlights the conclusion and recommendations pertaining to the advantages and disadvantages of the adopted methods, and makes suggestion for future work and future developments.

Chapter Six: All previous research works that have been cited in this study are acknowledged by complete references.

CHAPTER 2

Instrumental Methods of Analysis

2.1 Introduction

From the previous section, the corrosion of the alloys is the central theme in the application of these alloys to the oral environment. However, the susceptibility of a metal to corrosion depends on the (electrolysis) reduction–oxidation (redox) potential (E_h), measured in volts (V), $V \propto i$, of the metal. The current, i, is measured between a range of fixed potentials (voltages), V_1 to V_2. The three most often applied analytical techniques to investigate electrolysis mechanisms (voltammetry) are:

- Potential sweep voltammetry (PSV): the applied voltage is instantaneously moved (jumped) from one value V_1 to V_2. The resulting current is measured as a function of time, t;
- Linear sweep voltammetry (LSV): in this techniques the voltage range is also fixed, but the voltage is scanned for the lower voltage to the higher voltage. this renders LSV dependent on
  - the rate of electron transfer reactions,
  - the chemical reactivity of the active species, and
  - the rate with which the voltage is scanned and,
- Cyclic voltammetry (CV): CV is similar to LSV, with the exception that when the higher voltage is reached, then the scan is reversed and the voltage is swept back to the lower voltage.

Cyclic voltammetry (CV) has widely applied in the measurement of the extent of corrosion, especially in the instances where reversible reactions might occur; and this technique is applied in this study.

The composition of the alloy needs to be known to be able to discern which elements may have a marked influence on the corrosion. As corrosion is influenced by the concentration of the metals present, it is preferable that non–destructive methods of characterization should be used. X–ray emission spectroscopy is a non-destructive analytical technique in that the specimen can be analysed as is and does not have to be dissolved in aqueous or acidic media. The emission of X–rays can be induced by bombardment of particles such as electrons, protons and deuterium. in the bombardment with the heavier

(atomic mass) particles, some of the particles might be backscattered and would damage the window of a detector. This damage is prevented by placing a thick window in the detector. This prevention results in the emitted X-rays of the light elements such as C, N *etc.* are being absorbed in this window. Hence the light elements cannot be determined by bombardment with the heavy particles. Bombardment with electrons is therefore preferable and is the principle of scanning electron microscopy (SEM).

In the manufacture of alloys it is normally assumed that the elemental distribution is homogeneous. Undesired elements, which may adversely affect the anti–corrosion of the alloy, might have been introduced into the matrix. These metals might have given rise to metallic phases or crystallographic structures, which cannot be ascertain with CV or SEM. X-ray diffraction (XRD) is a non-destructive analytical technique that is applied in the identification of these crystallographic structures.

Corrosion may at times be visible on the surface of the alloy. there is however no indication of the extent of corrosion below the surface. Atomic force microscope (AFM) or scanning force microscope is a very high resolution type of scanning probe microscope, with the demonstrated resolution of fractions of nanometer. It is more than 1000 times better than the optical diffraction limit. In tapping mode, the cantilever is driven to oscillate up and down at near its resonance frequency by a small piezoelectric element mounted in the AFM tip holder (Binning *et al.*, 1986). The AFM has many advantages compared to scanning electron microscope (SEM). The electron microscope provides a two–dimensional projection or a two–dimensional image of a sample, the AFM provides a three–dimensional surface profile. The AFM has the disadvantage in image size compared to SEM. The SEM can image an area approximately square millimeters with a depth of field in the range of millimeters.

Secondary ion mass spectrometry (SIMS) is used to analyze surface layers of various materials used in biology and physics and is a standard micro analytical and imaging technique. SIMS based on the observation that charged particles (secondary ions) are ejected from the surface of a sample when bombarded by a primary beam of heavy particles. SIMS Image consists in bombarding under high vacuum a solid specimen with a beam of accelerated ions (primary ions) a few keV in energy. The physical interactions between the incident primary ions and the specimen surface involve complex processes of chemical bond breaking and atom recombination with the consequence that the most superficial atomic layers of the solid are sputtered out part of this material being in the form of monoatomic or polyatomic ions (the secondary ions). These secondary ions are collected and dispersed using a high performance mass spectrometer which enables specific secondary ions to be selected (Tafforeau *et al.*, 2002). These secondary ions which are sputtered from the bombarded area (less than 1 $mm^{2]}$ in the scanning mode) of the sample surface are counted using an appropriate device (electron multiplier) and the value obtained (i.e., the signal) is stored in the memory of a computer. The beam is raster over the surface of the sample to produce a 256×256 pixels digital image. Finally, the images are edited using grey-level or false-colour scales. The detection limit of the SIMS method is of the order of a few ppm for any isotope of most elements. This method is also characterised by an excellent mass resolution which makes it possible to

resolve most problems of mass interference (Tafforeau *et al.,* 2002).

2.2 Cyclic Voltammetry (CV)

The quantification of cyclic voltammetry data has been effected by using the Randles–Sevcik equation which describes the effect of scan rate on the peak current i_p [1]. This current is normally given in terms of the parameters n, A, F, D, C, ν, R, T, which are respectively the number of electrons transferred in the redox event, electrode area in cm^2, Faraday constant in $Cmol^1$, diffusion coefficient in cms^{-1}, concentration in $mol.cm^{-3}$, scan rate in Vs^{-1}, the universal gas constant in VCK^1mol^1 and temperature in K.

$$i_p = 0.4463nFAC\sqrt{\frac{nT}{RT}} \tag{2.1}$$

Considering now a conventional half cell reaction, as a reduction, where the electrons are on the left side of the equation, and the capital letters repesent the species and the small letters the stoiciometric coefficients, the raction can be written as: aA + bB + ne^- + hH^+ $\rightarrow$ cC + dD, the half cell standard potential, E_0 (volts), is expressed in terms of the change in Gibb's free energy, G^0, n, and F, by $E^0 = \frac{\Delta G^0}{nF}$. The actual potential, E, is then related to the pH and the concentration of the species [..] at ambient temperature, by

$$E = E_0 + \frac{0.05916}{n} log \frac{[A]^a[B]^b}{[C]^c[D]^d} - \frac{0.05916h}{n} pH \tag{2.2}$$

and consequently

$$E_h - E_0 = \Delta E = \frac{0.05916}{n} log \frac{[A]^a[B]^b}{[C]^c[D]^d} - \frac{0.05916h}{n} pH \tag{2.3}$$

Furthermore, the concentration at the electron depends on the flux, j, which is proportional to the concentration of the ionic species. Thus in terms of the C in the dolid phase, C_i, the content in the material, θ_s, and that in the minimal amount of liquid (in the pores), θ, the electricla potential, ϕ, the bulk velocity in the fluid,v_x, the chemical activity coefficient, γ_i, and valence number of the species, z_i the flux can be pxpressed by:

$$j_i = \alpha + \beta_1\beta_2 \times \beta_3 + C_iV_x \tag{2.4}$$

where $\alpha = -\theta D_i \frac{\partial C_i}{\partial x}$, $\beta_1 = -\theta \frac{D_i z_i F}{RT}$, $\beta_2 = C_i \frac{\phi}{\partial x}$ and $\beta_3 = \theta D_i C_i \frac{\partial \gamma_i}{\partial x}$. In addition, D_i normallly cited in literature, is the diffusion of the species in free water, and as such neglects the matrix in which the species is found. This can be overcome by including the tortuosity, τ, by expressing D_i as $D_i = \tau D_i^{\mu}$. Hence, maintaining the temperature and incorporating the equation of dE, the current in the cyclic voltammetric analysis will be pH dependent.

A plot of a typical voltammogram is shown in figure 2.1. Starting at an initial voltage at point A, and then the potential is scanned in the negative direction at B, the reaction continues at the electrode until most of the species has been reduced, peaking the cathodic current at point C. The rise in current is followed by decay for the rest of the forward scan until the potential scan is reversed at point D. The

[1] When R, F and T at 25^0C are in corporated, then the general equation is $i_p = 2.686 \times 10^5 AC\sqrt{n^3\nu D}$

scan in the positive direction proceeds similarly to that of the negative direction. The cathodic current continues to slowly decay until the potential reaches a point to start the oxidation of the species at point E.

The anodic current is then measured as being proportional to the concentration of the reduced species is significantly diminished at point F (Mohammad, 2014). The anodic current then decays from this peak, and the potential completes its cycle. The resulting plot of current versus potential is called a cyclic voltammogram. The important parameters in a cyclic voltammogram are the anodic and cathodic peak potentials, E_{pc} and E_{pa}, and anodic peak current (i_{pa}) and catholic peaks currents (i_{pc}) (Maoela, 2009).

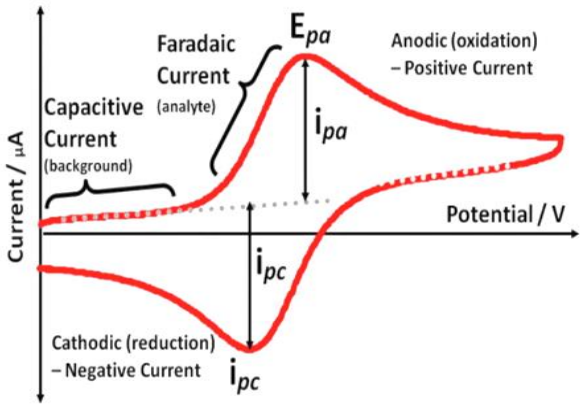

Figure 2.1: Plot a typical cyclic voltammogram, of the change in current as the voltage is increased, for an electrochemical reaction.

2.3 Scanning electron microscopy (SEM)

SEM uses a focused electron beam to image the surface. The image is obtained by scanning the focused electron probe across the surface and collecting the resulting image signal from the surface. The signal is collected from the specimen surface and the electron beam loses energy by inelastic scattering as the electrons penetrate beneath the sample surface. Most of the electron current from an excited sample is due to the release of secondary electrons from the sample surface (Brandon & Kaplan, 2008).

SEM images are produced by scanning the beam while displaying the signal from an electron mode. In many applications, the large depth of field in SEM images, typically at least 100 times greater than for a comparable optical microscope, is more relevant than the high resolution. An important factor in the success of SEM is that images of three-dimensional can be generated. The range of applications of SEM can be extended by adding other types of detectors (Reed, 2005). In a scanning electron microscope, a beam of electrons is produced at the top of the microscope by heating a metallic filament. The electron beam follows a vertical path through the column of the microscope. It makes its way through electromagnetic lenses which focus and direct the beam down towards the sample. Once it hits the sample, other electrons (backscattered or secondary) are ejected from the sample.

Detectors collect the secondary or backscattered electrons, and convert them to a signal that is sent to a monitor producing an image. The basic components of SEM are the lens system, the electron gun, the

electron collector, the visual and photo recording cathode ray tubes (CRTs) and the associated electrons as shown below. Some of the major reasons which make SEM one of the most useful instruments in a widely array of research fields today are: (1) High resolution on the order of 1–5 nm; (2) Large depth of focus; (3) Higher magnification and (4) Ease of sample observation. One of the most promising advances in the development of the SEM is the capability to determine the crystal structure and grain orientation of crystals on the surface of prepared samples. To do so, SEM requires vacuum resistant and conducting samples. One possible way to examine non conducting samples is to deposit a thin film of conducting material to reduce charging effects.

2.4 X–ray Diffraction (XRD)

X–Ray diffraction (XRD) is a versatile, non-destructive technique that reveals detailed information about the chemical composition and crystallographic structure of natural and manufactured materials (Cullity, 1978). X–ray diffraction methods have both qualitative and quantitative characteristics. Qualitative analysis involves the identification of phase or phases in a specimen by comparison with the reference pattern (i.e. data collected by someone else) and relative estimation of proportions of different phases in multiphase specimens by comparing peak intensities attributed to the identified phase. The quantitative analysis of diffraction data involves the determination of amounts of different phases in multi-phase samples. In quantitative analysis an attempt is made to determine structural characteristics and phase proportions with quantifiable numerical precision from the experimental data itself. The most successful quantitative analysis usually involves modeling diffraction pattern such that the calculated pattern(s) duplicates the experimental one.

All quantitative analysis requires precise and accurate determination of the diffraction pattern for a sample in terms of both peak positions and intensities. The phase identification using X-ray diffraction depends on the positions of the peaks in the diffraction profile with relative to intensities at some extent. Another important aspect of the diffraction technique from the material is to consider how diffraction peaks change through the presence of various types of defects such as small number of dislocations in crystals with dimensions in millimeters. The defects can be caused by the small grain size, which can change diffraction peak widths (Hussain, 2008).

2.5 Atomic force microscopy (AFM)

The atomic force microscope (AFM) or scanning force microscope is a very high resolution type of scanning probe microscope, with the demonstrated resolution of fractions of nanometer. It is more than 1000 times better the optical diffraction limit. In tapping mode, the cantilever is driven to oscillate up and down at near its resonance frequency by a small piezoelectric element mounted in the AFM tip holder (Binning *et al.*, 1986). The AFM has many advantages compared to scanning electron microscope (SEM).

The electron microscope provides a two-dimensional projection or a two–dimensional image of a sample, the AFM provides a three-dimensional surface profile. The AFM has the disadvantage in image size compared to SEM. The SEM can image an area approximately square millimeters with a depth of field in the range of millimeters. The AFM can only image a maximum height approximately micrometers and a maximum scanning area of around 150 $\times$ 150 micrometers (Martin *et al.*, 1987; Binning *et al.,* 1986).

2.6 Secondary ion mass spectrometry (SIMS)

Secondary ion mass spectrometry (SIMS) is used to analyze surface layers of various materials used in biology and physics and is a standard micro analytical and imaging technique. SIMS based on the observation that charged particles (secondary ions) are ejected from the surface of a sample when bombarded by a primary beam of heavy particles. SIMS Image consists in bombarding under high vacuum a solid specimen with a beam of accelerated ions (primary ions) a few keV in energy. The physical interactions between the incident primary ions and the specimen surface involve complex processes of chemical bond breaking and atom recombination with the consequence that the most superficial atomic layers of the solid are sputtered out part of this material being in the form of monoatomic or polyatomic ions (the secondary ions). These secondary ions are collected and dispersed using a high performance mass spectrometer which enables specific secondary ions to be selected (Tafforeau *et al.*, 2002).

These secondary ions which are sputtered from the bombarded area (less than 1 mm^2 in the scanning mode) of the sample surface are counted using an appropriate device (electron multiplier) and the value obtained (i.e., the signal) is stored in the memory of a computer. The beam is raster over the surface of the sample to produce a 256$\times$256 pixels digital image. Finally, the images are edited using grey–level or false–colour scales. The detection limit of the SIMS method is of the order of a few ppm for any isotope of most elements. This method is also characterised by an excellent mass resolution which makes it possible to resolve most problems of mass interference (Tafforeau *et al.,* 2002).

The secondary atomic and molecular ions are extracted with electric fields and then separated and detected in a mass analyzer Depending on the type of mass analyzer, one discerns between either conventional SIMS, with magnetic or quadrupole mass spectrometers, or TOF–SIMS, with time–of–flight mass spectrometers. TOF–SIMS Contrary to this, time–of–flight mass spectrometry allows to measure all secondary ions with one polarity quasi–simultaneously. The sample is bombarded in TOF–SIMS with a short–time primary ion pulse with typical lengths between several hundred picoseconds and a few nanoseconds. This is repeated every few hundred microseconds, resulting in a duty cycle of typically 10–5 (Stephen, 2001).

CHAPTER 3

Materials and Methods

3.1 Materials

3.1.1 Alloy preparation

Three dental alloys PD CASTA–H, CERACAST–NB, and PD–2000, were obtained from Mountain Medico Company, Upland (California), USA. The materials were received in the cylinder–form with diameter of 7mm and 15mm length. The alloys were cut into lengths of 3 mm, with the diameter size maintained. The manufacturer's certificate of compositional analysis of the three alloys are given in table..

Figure 3.1: Three dental alloys PD CASTA–H, CERACAST–NB, and PD–2000, were obtained from Mountain Medico Company, Upland (California), USA. The materials were received in the cylinder–form with diameter of 7mm and 15mm length.

3.1.2 Alloy treatment

The alloys were divided into 6 groups. Each group contained three different alloys from each type.

All samples from each group were tested in artificial saliva solution, for 14 days. T The pH of the

solution was measured before the experiment using a glass electrode (Model pH 25, Manusl, Spain) pH meter. The pH of the solution was reduced 8 to 4-5 by adding lactic acid. This acid was chosen in order to obtain conditions that were as close as possible to the clinical reality, since this acid is naturally released by the bacteria in the buccal cavity (Grimsdottir,1993; Schiff et al., 2002). All the samples were kept at fixed temperatures (28^0C, 37^0C) inside the Incubator (Scientific- series 2000) for 14 days. However, for higher temperature the samples were kept in the Oven (Labotec-term-o-Mat30-250^0C) set at 40^0C.

3.1.3 Ringers corrosion solution

The chemicals needed for the preparation of the Ringers solution, NaCl, $CaCl_2$, KCl and $NaHCO_3$ (Sutow *et al.*, 2010) were sourced locally through the companies B&M Scientific, Lasec Laboratories and Industrial Analytical. All the chemicals were of analytical grade quality. The solution was prepared from stoiciometic amounts of the chemicals indicated above. The solution was stirred using magnetic stirrer until all content are completely dissolved , the solution was refridgerated (4^0C) until used. The preparation of the solution was done at Radiology LABS, at iThemba LABS, Western Cape, South Africa.

3.2 Methods: Analytical Techniques

3.2.1 Cyclic voltammetry

The CV is a type of voltammetric techniques which uses to analyze new processes that take place at the surface of the electrode giving indications on the reversibility, the kinetics, and the different thermodynamic parameters of the process (Mohammad, 2014). The CV uses to study of redox processes, for understanding reaction intermediates and for obtaining stability of reaction products. The potential can be cycled between the two switching potential for several cycles before the experiment is ended at the final potential (Gosser, 1993).

The corrosion test cell was used was located in the Chemistry Department, University of the Western Cape, South Africa. The dental alloys were cleaned for two minutes by using distilled water. One litter of Ringers corrosion solution, pH = 2.5, 6.5, and the temperature 37 $\pm$ 1 ^{0}C was used. The alloys were placed in the cell, the open circuit potential (Er) was monitored for 1 hour. All the cyclic voltammetry measurements in this study were carried out using a scan rate of 5 mVs^{-1}.

3.2.2 Scanning electron microscopy (SEM)

The scanning electron microscopy SEM (Auriga Carl Zeiss, Germany) was used to study the surface morphology, chemical composition and crystalline structure of dental alloys. The SEM used in the housed Physics Department at University of the Western Cape. South Africa. In SEM analysis, a focused beam of high-energy electrons with high vacuum is used, to generate a variety of signals at the surface of solid samples, the signals that derive from electron sample interactions reveal the information about the sample

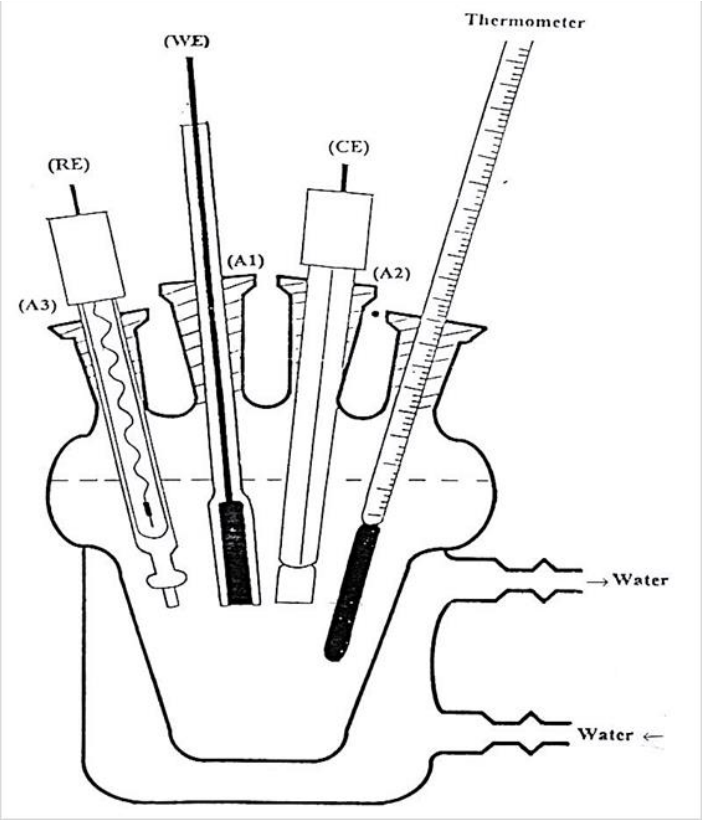

Figure 3.2: The corrosion test cell for cyclic voltammetry that was used in this study.

(Figure 3.5). Elemental mapping and atomic composition of the alloys were performed using Energy Dispersive X-ray Spectroscopy (EDS). Which is interfaced with SEM.

3.2.3 X-ray diffraction analysis (XRD)

X–ray diffraction instrument was used to characterize the crystalline structure and phases of three different dental alloys. A Bruker D8 Advance XRD instrument with Cu Kα source and wavelength of 1.54 angstrom was used at the Material Research Department (MRD), iThemba LABS, Western Cape, South Africa. This equipment uses a Vantec 2000 detector to determine wide diffraction angles of the material with a powerful non–destructive. It also provides details and information of the composition, characterizing crystalline structure, phases of solid materials, and other structural parameters, such as average grain size, crystallinity, strain, and crystal defects X-ray diffraction peaks. X-ray diffraction technique has been utilized to detect changes in crystalline and amorphous regions along with the degree of crystallinity. As x-rays are predominantly diffracted by electron density, analysis of the diffraction angles can be used to produce an electron density map of a given crystal or crystalline structure (Rana et al., 2009).

3.2.4 Atomic force microscopy (AFM)

The AFM was used to study the surface morphology of three different dental alloys and provides a 3D profile of the surface on a nanoscale, by measuring forces between a sharp probe (<10 nm) and surface at

Figure 3.3: Photograph of the scanning electron microscopy SEM (Auriga Carl Zeiss, Germany) used in this study.

very short distance (0.2-10 nm).

AFM is a very sensitive technique with high-resolution surface imaging by scanning a sharp probe over the surface of a specimen. The Gwyddion software, version 2.36, was used to translate the data of the high resolution 3–D surface images of the alloys. The AFM analysis was done in the Department of Electrical and Electronic Engineering, University of Stellenbosch, Western Cape, South Africa.

3.2.5 Time-of-flight secondary ion mass spectrometry (TOF-SIMS)

The TOF-SIMS was used for elemental and molecular surveys, mass spectrum graphs, surfaces and depths of the alloys. The instrument can measure concentrations up to parts per billion (ppb). The SIMS machine focused at a surface area about 1 millimetre and it operates extreme under vacuum of 10-9 Torre (Stephan, 2001). The TOF–SIMS model system used in the ion TOF SIMS5, with source: spectroscopy: Bi^{1+}, 1pA, 10KHz (100 μs), 30kV, with sputter area: $1000\mu \times 1000\mu$, resolution: 512×512 pixels. It has a detection limit in ppm to ppb range, and depth profiling <10nm. The TOF–SIMS data was obtained from the University of the Free State, Department of Geology, Bloemfontein, South Africa. In TOF–SIMS the samples did not need to be polished or coated. However, the surfaces were cleaned with an oxygen gun and charging was removed with a flood gun.

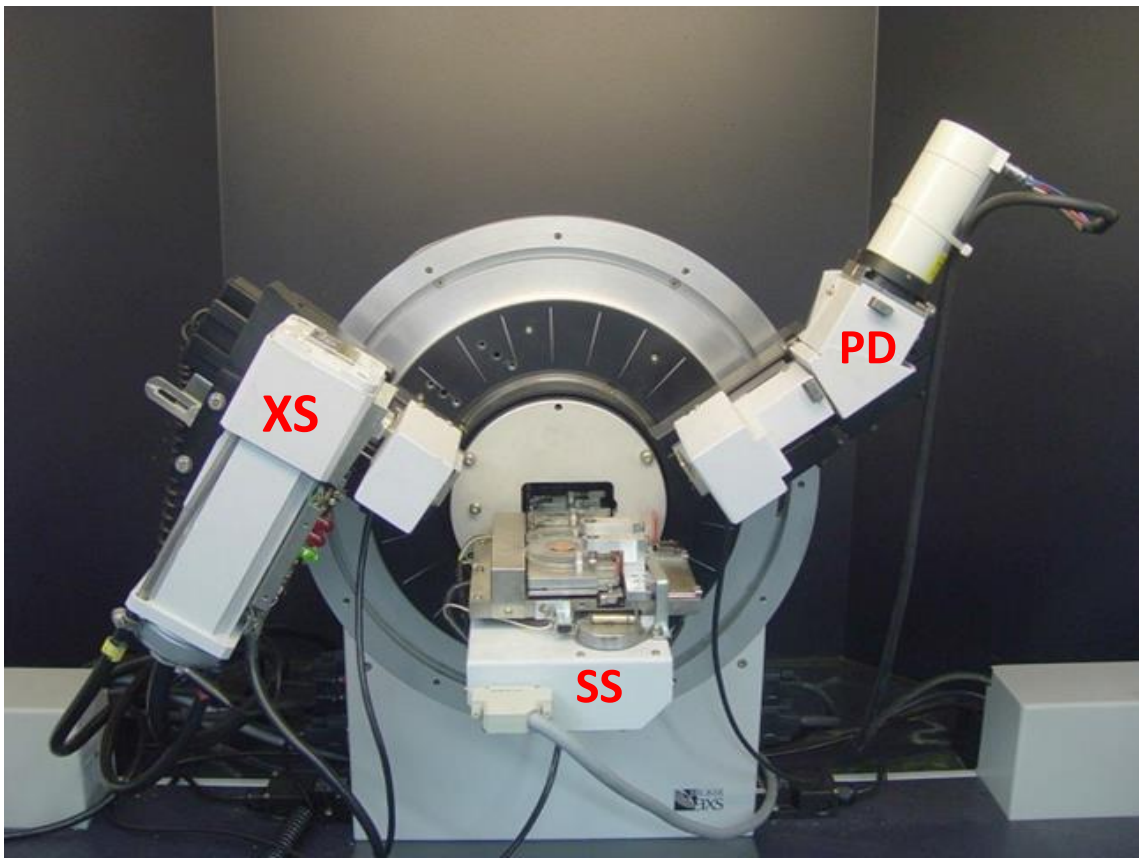

Figure 3.4: Photograph of the Bruker D8 Advance XRD instrument with Cu Kα source and wavelength of 1.54 angstrom was used in this study.

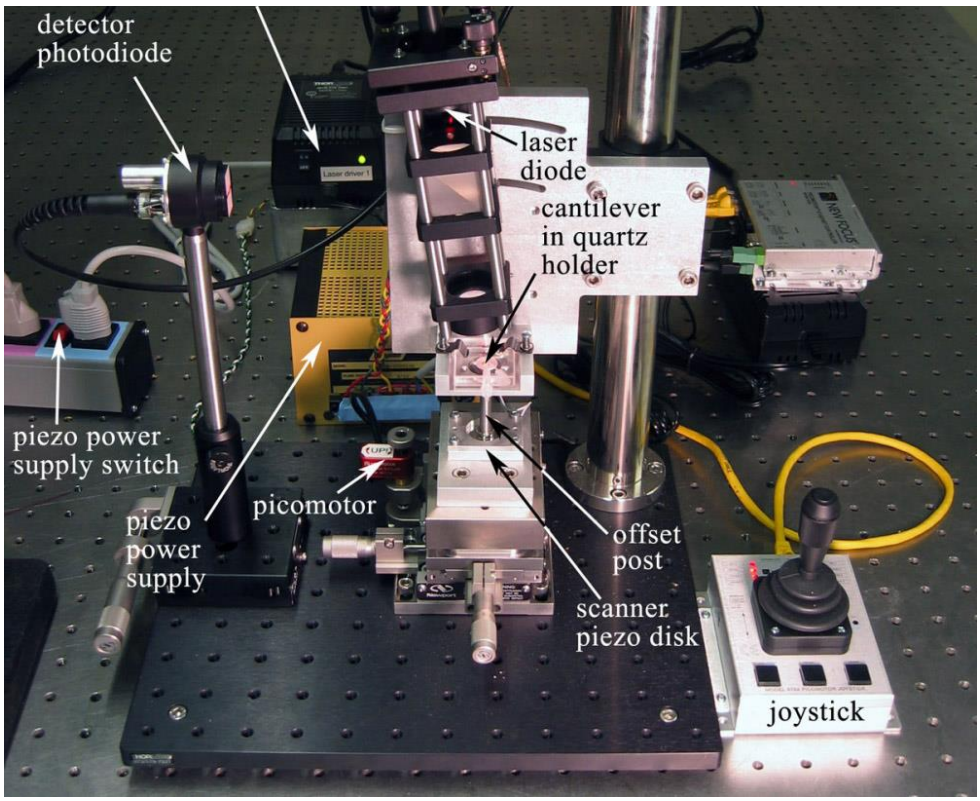

Figure 3.5: Annotated photograph of the AFM instrumentation.

3.2.6 Auxillary Equipments

Various equipments were used in the preparation of the solutions. These included:

The pH meter (Model pH 25, Manusl, Spain), was used to measure the pH (acidity or alkalinity) of the solution. It consists of a special measuring probe, a glass electrode connected to an electronic meter that measures and displays the pH reading.

Magnetic stirrer: The Corning PC351 hot plate magnetic stirrer consists of precise liquid temperatures and stirring speeds. It has temperature accuracy within $\pm 2^0 C$ and stirring speeds at $\pm$ 5%.

Analytical weighing balances: The weighing balances was (BRANCHES- Sartorius, NVS/WNNR). The balance was used to measure the weights of the chemical materials used in this study. The measuring pan of this balance installed inside transparent enclosure with doors, to ensure that no dust collected, and with no air currents in the room which will interfere with the balance operation and the sample measurement.

Oven: The Labotec (term-o-Mat 30-250^{0}C) oven was used to set higher temperatures, 40^{0}C.

Incubator: The Scientific Series 2000 laboratory incubator was chosen to set temperatures, 28^{0}C and 37^{0}C.

CHAPTER 4

Results and Discussions

4.1 Introduction

This chapter presents the experimental results and discussion, from three different dental alloys tested in artificial saliva (solution), at different pH value and temperatures. The presentation of the experimental analysis of sample surfaces, and the structure, particle morphology and the chemical composition were determined using numbers of analytical techniques which include: XRD, SEM, EDS, AFM, and SIMS. The electrochemical measurement was done using cyclic voltammetry (CV).

4.2 Cyclic Voltammetry

Electrochemical measurements were performed in a three–electrode corrosion cell at temperature of 37 $\pm$ 0.1^0C. A saturated calomel electrode (SCE) was used as reference electrode, platinum was used as counter–electrode and Ni–Cr and Co–Cr samples was used as working electrode, controlled by a personal computer with dedicated software (Volta Master 4) which was used to measure and analyse corrosion quickly, reliably and easily using cyclic voltammetry (CV). The analyses were performed on the three dental alloys: PD CASTA H (Cr–Co), CERACAST NB (Ni–Cr) and PD 2000. The corrosion resistance for each alloy was evaluated in Ringers solution at pH values of 6.5 and 2.5. The cyclic voltammetry data analysis were performed at a potential varying from -1000 mV/SCE to +1000 mV/SCE. The scan rate of 5 mVs^{-1}.

In fig 4.1 the cyclic voltammograms for PD CASTA H (Cr–Co) alloys recorded at a scan rate of 5 mV s^{-1} and 37^0C in Ringers solution at pH = 2.5 and 6.5 are presented. The potential scan was from -1.000 V to 1.000 V. In the presence of air, chromium metal spontaneously forms a layer of passive oxide of Cr_2O_3. The chemical equations for the formation of Cr_2O_3 at the electrode surface and its further oxidation to the chromate, CrO_4^{2-} at higher potentials leading to the recorded anodic peak, are presented in Chapter 2 (Kovačević *et al*, 2012). There was no significant variation in the voltammograms shapes with rspect to the pH values. The current density for the passive range is slightly higher at pH 2.5 and decreases at higher pH 6.5 (fig 4.1).

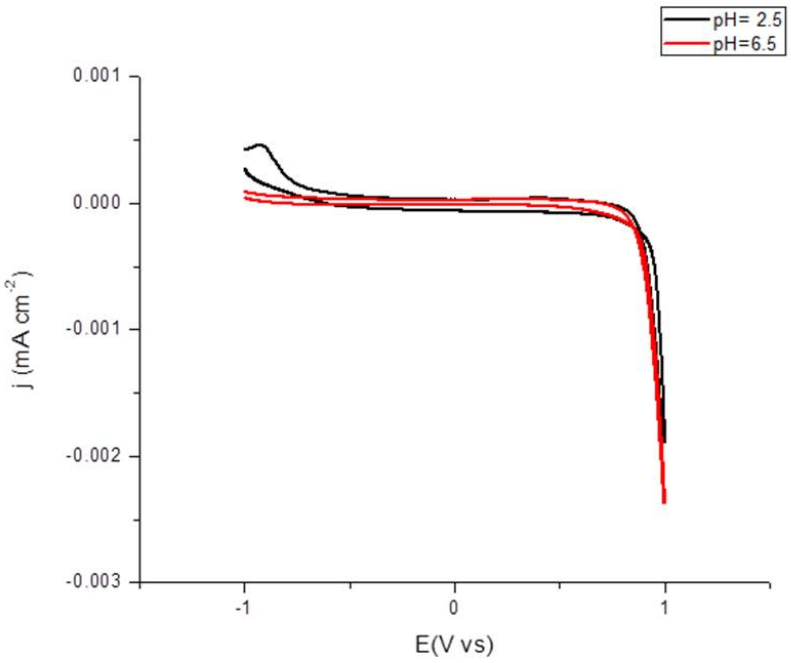

Figure 4.1: The combined cyclic voltammograms of the PD CASTA H (Cr–Co) alloy after immersion for 60 minutes in Ringers solution, pH values of 2.5 and 6.5, respectively. The voltammograms were recorded at a scan rate of 5 mVs^{-1} and the potential was varied form -1.000 V to 1.000 V. The temperature was maintained at 37^0C.

The combined cyclic voltammograms of the CERACAST NB (Ni–Cr) alloy after immersion for 60 minutes in Ringers solution, pH values of 2.5 and 6.5, respectively, are shown in fig4.2. The voltammograms were recorded at a scan rate of 5 mVs^{-1} and the potential was varied form -1.000 V to 1.000 V. The temperature was maintained at 37^0C. In the anodic range two peaks, A1 and A2, are visible. These peaks are related to the formation of NiO on the surface. In the reverse scan, at ≈0.5V, there was small cathodic peak, K1, appears, which is related to the reduction of Ni (VI) to Ni (III). The chemical equations for the cathodic and anodic peaks are represented by the reactions indicated in chapter 2 (Kovačević *et al.*, 2012). From the results in fig. 4.2, the anodic peak A1 at pH 2.5 appeared at ≈0.4 V where the pH value was lower. The second anodic peak A2 appears at ≈0.3 V in the solution at pH 2.5. These peaks are related to the oxidation of Ni (II) oxide to Ni (III) oxide.

At high alkali concentration, this is electrochemically-formed NiO because the OH^- ions activate the Ni–Cr surface, which is evident by the increase of the anodic current density as the peak height as the concentration of alkali (NaOH) increases. Generally, there is a trend of decreasing current density with increasing pH value due to the formation of more stable oxide layers at neutral and slightly alkaline solutions.

In PD 2000 free–Ni alloys, the cyclic voltammograms were recorded in the potential range from -1.000 V to 1.000 V (see fig4.3). The electrochemical behaviour of this alloy is very similar to that of PD CASTA H (Cr–Co) alloys, with an anodic peak A1, which may release to the formation of Cr_2O_3 at the

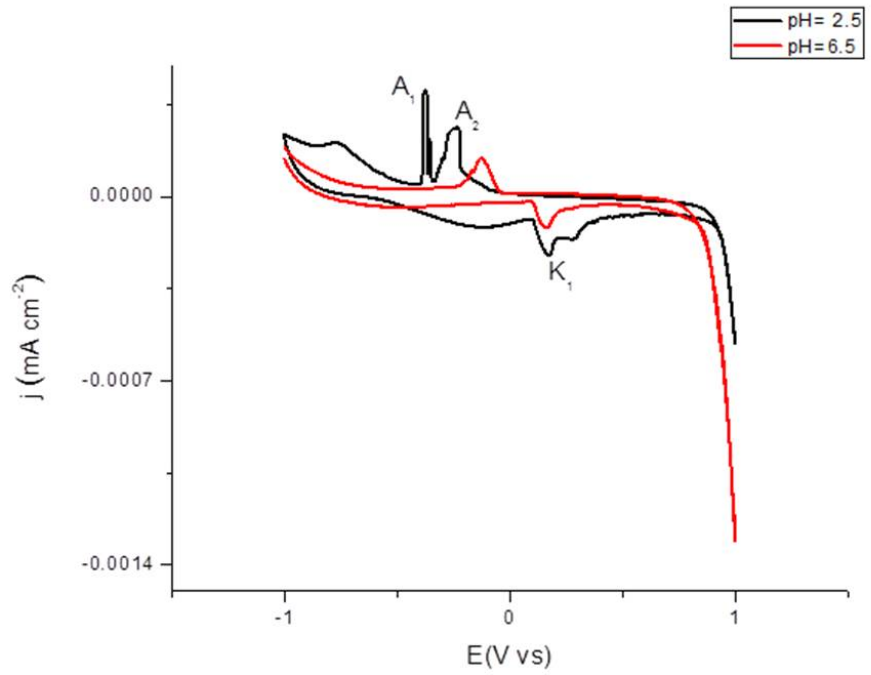

Figure 4.2: The combined cyclic voltammograms of the CERACAST NB (Ni–Cr) alloy after immersion for 60 minutes in Ringers solution, ph values of 2.5 and 6.5, respectively. The voltammograms were recorded at a scan rate of 5 mVs^{-1} and the potential was varied form -1.000 V to 1.000 V. The temperature was maintained at 37^0C.

electrode surface and its further oxidation to CrO_4^{2-} at higher potentials leading to the recorded anodic peak as for PD CASTA H alloy. The change in pH value of the solution does not significantly affect the electrochemical behaviour of Cr–Co alloys.

4.3 Scanning Electron Microscopy (SEM) Analysis

4.3.1 Micrographs of surface morphologies

4.3.1.1 Determination of the surface morphologies before the corrosion test

The determination of the surface topography was done before the immersion in the solution using SEM (Carl Zeiss Auriga, Germany). The three samples (alloys) were carefully cleaned with alcohol, and then dried by the air drier before SEM analysis. The surface morphologies of the alloys are shown in figure 4.4. There is no corrosion observable on the surfaces of the alloys in initial state.

4.3.1.2 Determination of the surface morphologies of alloys after the test Ringers solution at pH 6.5 and 37^0C

The Ringers solution used was at pH 6.5 and the temperature was maintained at 37^0C. The surface topography of the samples were determined using SEM. The micrographs have shown that pitting corrosion at different areas on the surface of PD CASTA H, CERACAST NB and PD 2000 (see figure

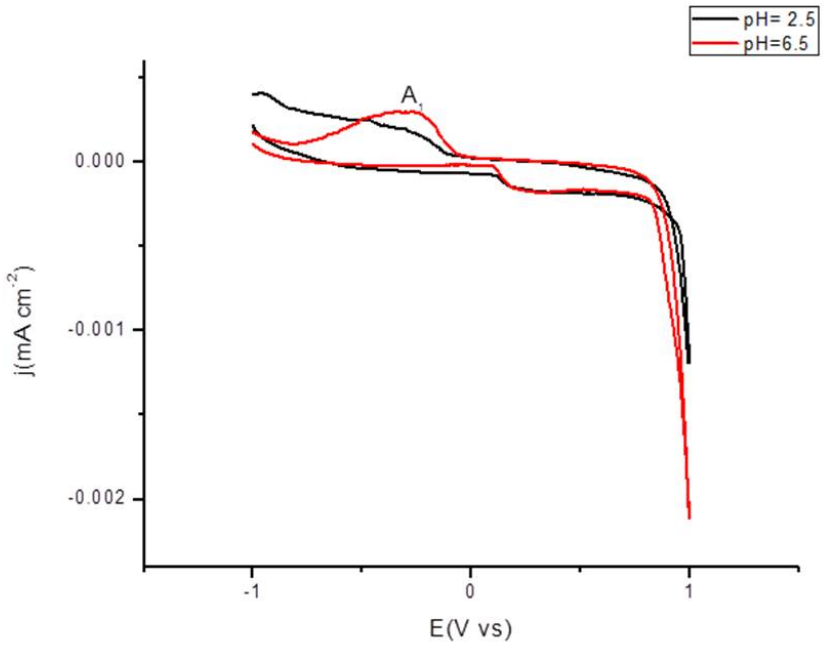

Fig ers
sol

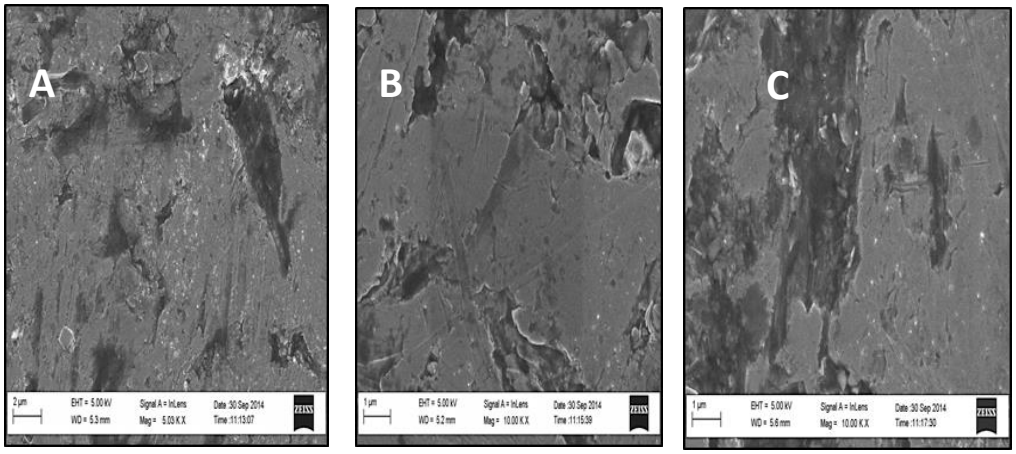

Figure 4.4: Surface morphologies of the (A) Co–Cr–Ni alloy, (B) Ni–Cr alloy and (C) Co–Cr free Ni alloy, before immersion into the Ringers test solution.

4.3.1.3 The surface morphologies for the alloys on Ringers solution pH 6.5 and at 28^{0}C

The surface morphologies of (a) Co–Cr–Ni alloy, (b) Ni–Cr alloy, (c) Co–Cr free Ni alloy by SEM, after immsersion into the Ringers test solution at pH 6.5 and at 28^{0}C are shown in figure 4.6.

4.3.1.4 The surface morphologies for the alloys on Ringers solution pH 6.5 and at 40^{0}C

The Ringers solution was set at pH 6.5 and the temperature increased to 40^{0}C. In this manner the effect of the higher temperature on corrosion resistance of Co-Cr and Ni–Cr alloys could be determined.

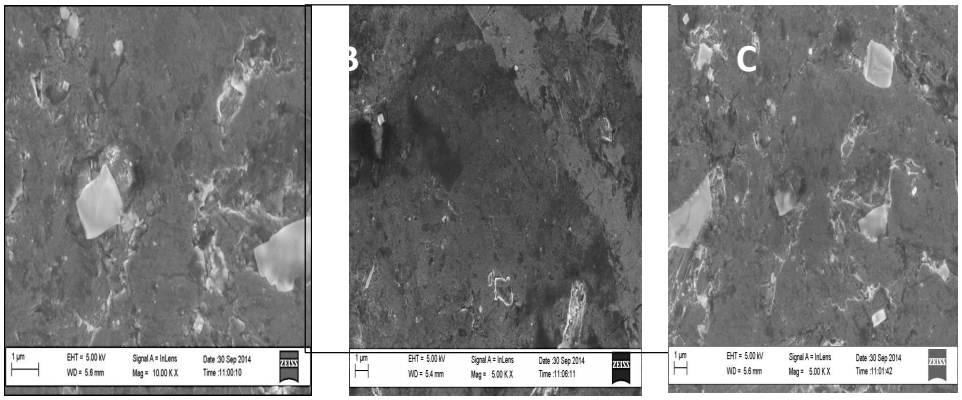

Figure 4.5: Surface morphologies of (A) Co–Cr–Ni alloy, (B) Ni–Cr alloy and (C) Co–Cr free Ni alloy, after immersion into the Ringers test solution at a pH of 6.5 and temperature of 37^0C.

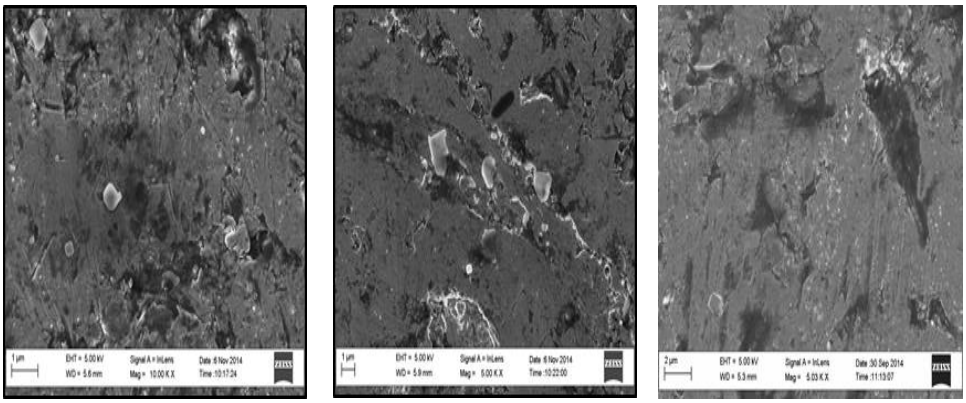

Figure 4.6: Surface morphologies of (A) Co–Cr–Ni alloy, (B) Ni–Cr alloy and (C) Co–Cr free Ni alloy, after immersion into the Ringers test solution at a pH of 6.5 and temperature of 28^0C.

in figure 4.7 is shown the corrosion on the surface of Cr-Co and Ni-Cr alloys. As the change in the temperature happens during the in–take of different foods and liquids, one of the oral conditions is related to degradation of alloys in the mouth which may have an effect on corrosion resistance. From this results the corrosion resistance of PD CASTA H, CERACAST NB and PD 2000 alloys was decreased with increasing the temperature of the solution to 40^0C. It is accompanied by a decrease in oxygen concentration of the solution (Bennani *et al.*, 2008).

4.3.1.5 The surface morphologies for the alloys immersed into Ringers solution pH 2.5 and at 28^0C

The pH of the solution was reduced to 2.5, by adding lactic acid, $C_2H_4OHCOOH$. The effect of these parameters on the surface morphologies is shown in figure 4.8. There are differences in the extent of corrosion on all the three dental alloys when the pH of the solution was reduced to 2.5. The CERACAST NB (Figure 4.12 b) exhibited the lowest corrosion resistance compared with that of PD CASTA H and

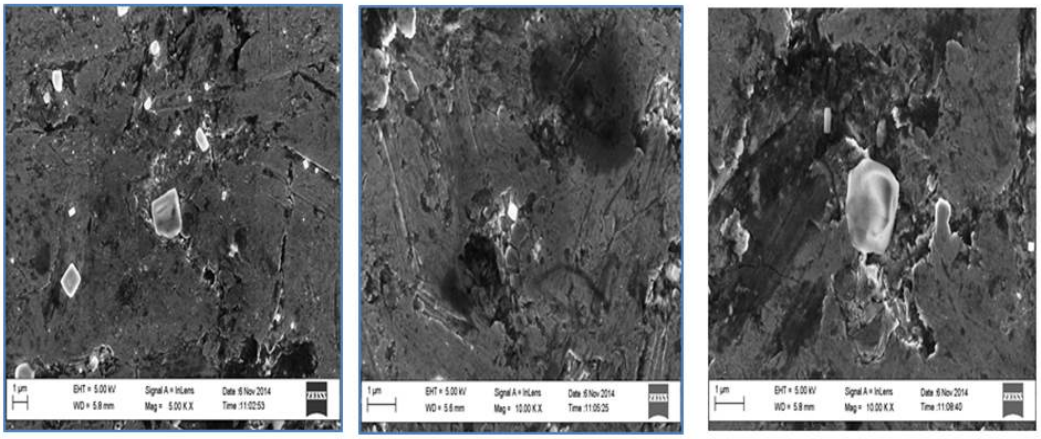

Figure 4.7: Surface morphologies of (A) Co–Cr–Ni alloy, (B) Ni–Cr alloy and (C) Co–Cr free Ni alloy, after immersion into the Ringers test solution at a pH of 6.5 and temperature of 40^0C.

PD 2000. It is important to assess the corrosion behavior of dental alloys in acidic solutions due to the variable pH conditions routinely encountered in the oral environment through the variety of foods and liquids ingested (Al Subari et al., 2013).

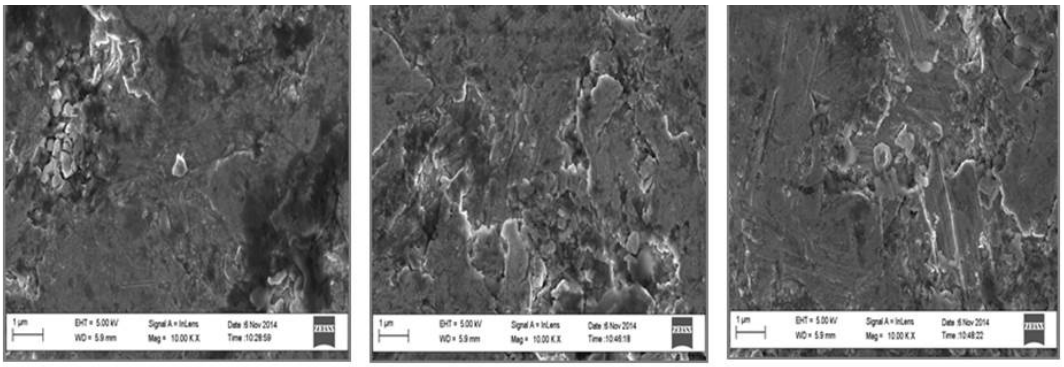

Figure 4.8: Surface morphologies of (A) Co–Cr–Ni alloy, (B) Ni–Cr alloy and (C) Co–Cr free Ni alloy, after immersion into the Ringers test solution at a pH of 2.5 and temperature of 28^0C.

4.3.1.6 The surface morphology for the alloys on Ringers solution pH 2.5 and at 40^0 C

The increase the pH and temperature had a marked effect on the alloys. The micrographs of the surface morphologies (see figure 4.9) show that the corrosion resistance of the tested alloys was decreased with increased the temperature of the Ringers solution to 40^0C. This might be due to a decrease in oxygen concentration of the solution .

4.3.2 Energy Dispersive Analysis of emitted X-rays (EDAX)

In this study a silicon ultra–thin window (SUTW) detector was interfaced with the scanning electron microscopy for detection of the X-rays emitted by the elements that comprise the alloys. The accelerating

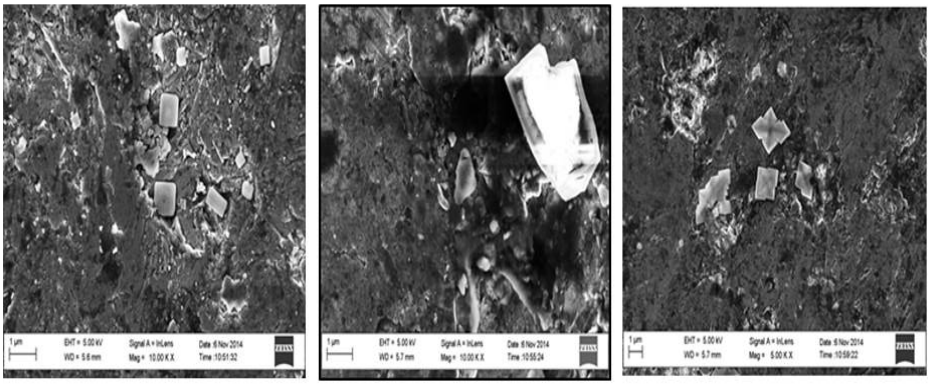

Figure 4.9: Surface morphologies of (A) Co–Cr–Ni alloy, (B) Ni–Cr alloy and (C) Co–Cr free Ni alloy, after immersion into the Ringers test solution at a pH of 2.5 and temperature of 40^0C.

energy of the electron beam was 20keV. The alloy was irradiated for a time period of 120 seconds. The dead–time correction was less than 10%. These experimental parameters were applied throughout the determination of the composition of the three alloys. The plot of the X-ray data as a spectrum of the PD

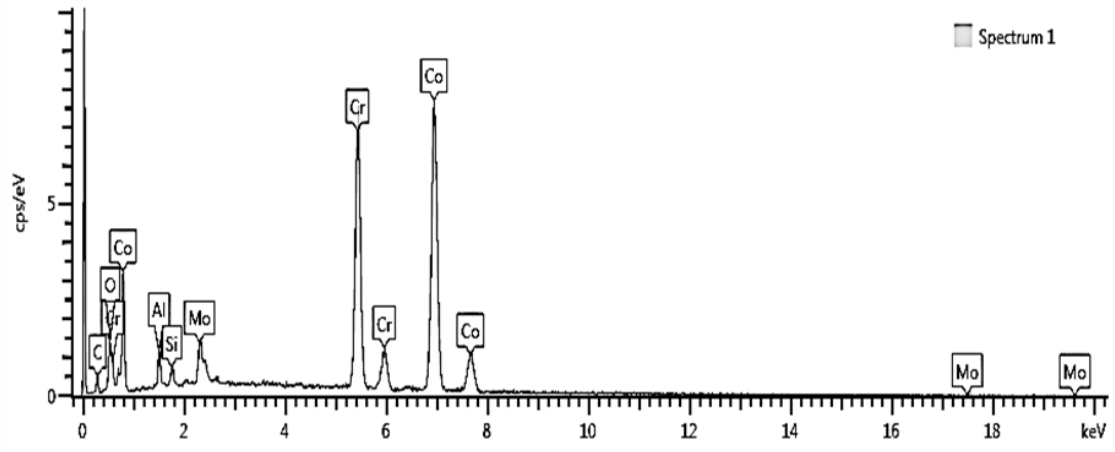

Figure 4.10: Plot of the X-ray data, as a spectrum, of the PD CASTA H (Co–CR) alloy. The accelerating energy of the electron beam was 20keV. The emitted X-rays were detected with a silicon ultra–thin window (SUTW) detector. The irradiation life time was 120 seconds.

CASTA H (Co–CR) alloy is shown in figure 4.10. Based on the X-ray data, plotted as different peaks, the elements present in the matrix of the alloy are Co, Cr, C, Mo, Si, Al and O. The sharp peaks of the Cr and Co K_α and K_β X-rays are clearly visible and show that the alloy has a higher content of Co and Cr when compared to another elements. The plot of the X-ray data as a spectrum of the CERACAST ND (Ni–Cr) alloy is shown in figure 4.11. Based on the X-ray data, plotted as different peaks, the elements present in the matrix of the alloy are Co, Cr, C, Mo, Si, Al and O.

The plot of the X-ray data as a spectrum of the PD 2000 (Co–Cr free Ni) alloy is shown in figure 4.12. Based on the X-ray data, plotted as different peaks, the elements present in the matrix of the alloy are Co, Cr, C, Mo, Si, Al and O. Figure 4.5: The EDS spectrogram of PD CASTA H (Co–Cr) alloy

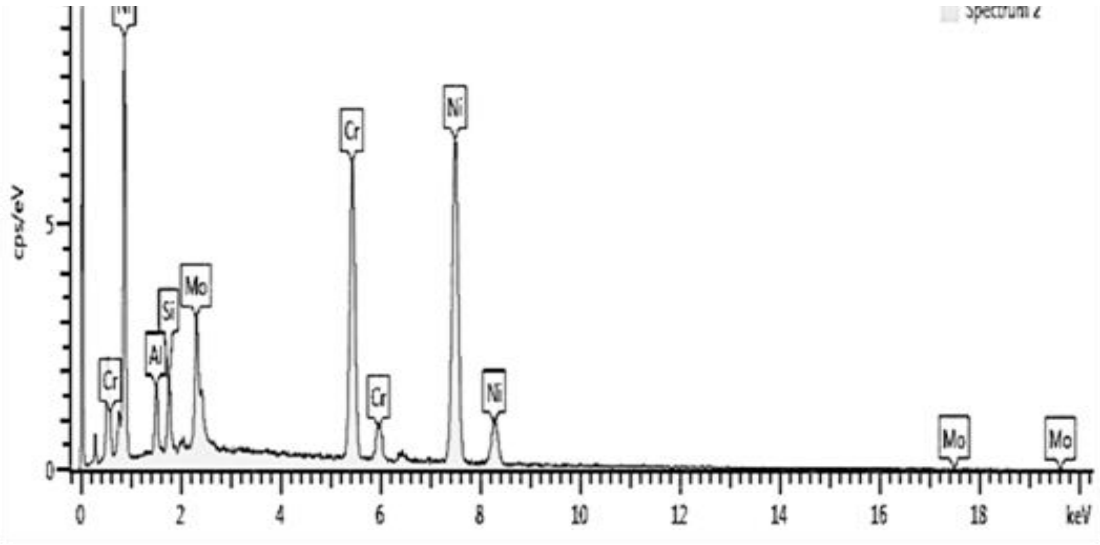

Figure 4.11: Plot of the X-ray data, as a spectrum, of the CERACAST ND (Ni–Cr) alloy. The accelerating energy of the electron beam was 20keV. The emitted X-rays were detected with a silicon ultra–thin window (SUTW) detector. The accelerating energy of the electron beam was 20keV and the irradiation life time was 120 seconds.

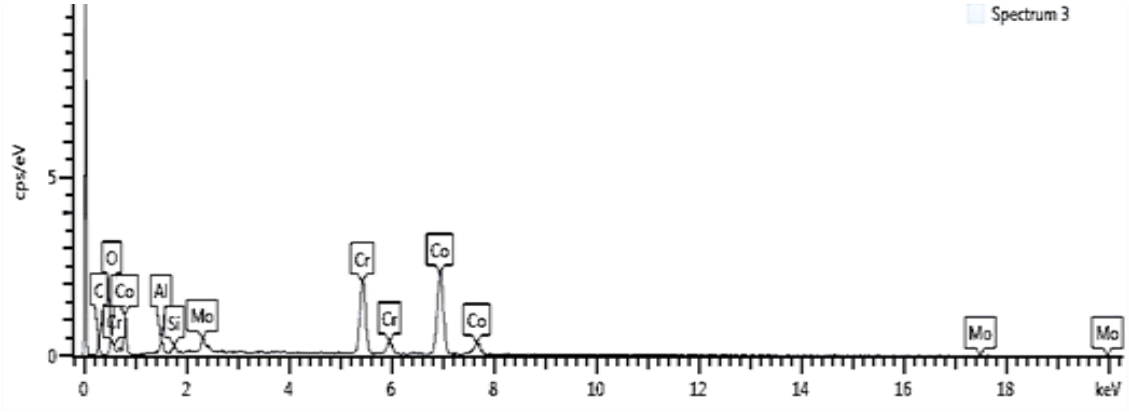

Figure 4.12: Plot of the X-ray data, as a spectrum, of the CERACAST ND (Ni–Cr) alloy. The accelerating energy of the electron beam was 20keV. The emitted X-rays were detected with a silicon ultra–thin window (SUTW) detector. The accelerating energy of the electron beam was 20keV and the irradiation life time was 120 seconds.

The EDAX spectrum in figure 4.11 shows that the alloy has a higher content of Ni and Cr, but a lower content of Al, Mo and Si.

The EDS spectrum, figure 4.12, of PD 2000 (Co–Cr free Ni) alloy showed the higher peaks of Co and Cr, with no peak for Ni, which indicates that the alloy is Ni–free. The elements with lower content are Mo, Si, O, and C.

There were significant differences in the percentage compositions of the constituent elements of alloys that have been studied before the immersion test compared with the results obtained from EDAX spectra after the test solution. This is perhaps due to the interplay between the ions of elements in the alloy and the ions of elements in the solutions during immersion period, or the effects of the pH and temperature of

Table 4.1: Comparison of chemical composition for the alloys given by the manufacturers and the chemical composition of the alloys obtained from the EDAX spectra after corrosion test by immersion in the Ringers solution. ND indicates not determinable.

Alloy	Cr	Co	Ni	C	Si	Mg	O	Al	Fe	Mo
PD CASTA H	29.00	60.00	2.00	ND	<1%	ND	ND	ND	2.00	6.20
CERACAST NB	25.00	<1%	61.00	ND	1.50	ND	ND	<1%	<1%	10.50
PD 2000	28.50	63.00	ND	<1%	<1%	<1%	ND	ND	ND	6.00
PD CASTA H	20.82	37.04	ND	12.94	1.39	ND	8.49	3.28	ND	2.04
CERACAST NB	26.71	ND	57.23	ND	4.48	ND	ND	5.99	ND	5.60
PD 2000	22.35	39.72	ND	10.96	1.55	ND	10.13	3.13	ND	216

the solutions (see table 4.1).

A comparison of chemical composition for the alloys given by the manufacturers and the chemical composition of the alloys obtained from the EDS spectrogram after corrosion test, is given in table 4.1.

4.4 X-ray diffraction analysis of alloys

The XRD experiments were carried out to complement the SEM measurements in order to identify the phases present in the microstructure of the alloy. The experiments were performed in an X–ray diffractometer Bruker D8 Advance, 2θ from 20^0 to 100^0, using the Cu–K_α radiation and wavelength of 1.54 . The phases were identified with the Origin–Pro 8 software. Three samples from each alloy were investigated by XRD before the testing solution.

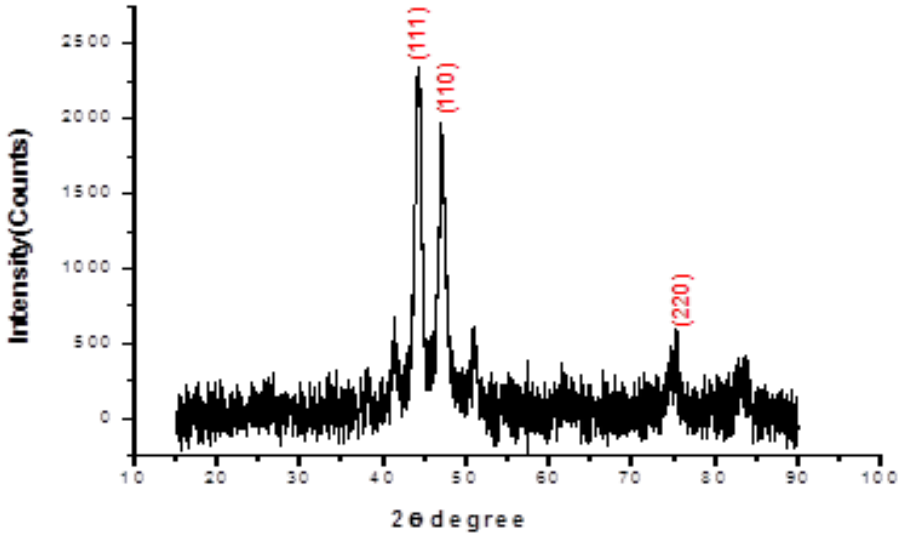

Figure 4.13: Plot of the X-ray diffraction data, as a spectrum, of the PD CASTA H (Co–Cr) alloy.

The plot of the X-ray diffraction data, as a spectrum, of the PD CASTA H (Co–Cr) alloy is shown in figure 4.13, with distinct diffraction peaks, identified to the (111), (110), (220). The lattice planes reveal that the as–prepared nanocrystals have a cubic structure. As seen in figure 4.13, the (111 Co) reflection

is the strongest peak. All the peaks were different, some were sharp and others broad. If the peak is

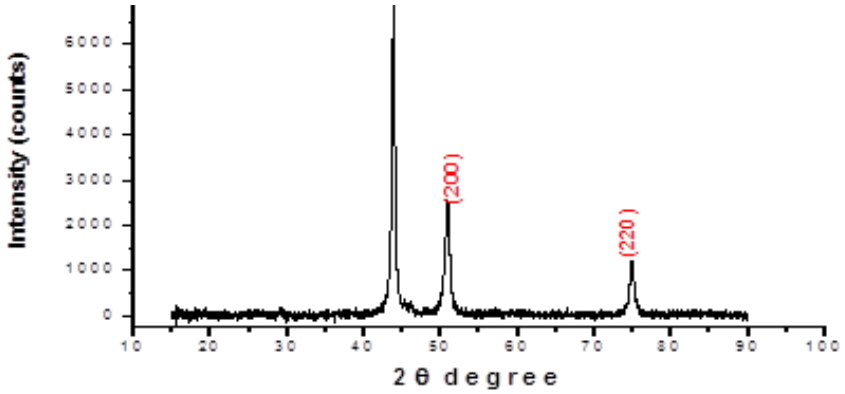

Figure 4.14: Plot of the X-ray diffraction data, as a spectrum, of the CERACAST NB (Ni–Cr) alloy.

sharp the full width at half maximum (FWHM) is small and the grain size is large. However, if the peak was broad, the grain size will be small and FWHM large. Therefore, the Cr–Co alloy has the mixture of large and small grains. In figure 4.14 is shown the plot of the X-ray diffraction data, as a spectrum, of CERACAST NB (Ni–Cr) alloy. XRD patterns with distinct diffraction peaks, identified to be (111), (200), (220), and lattice planes have face-centered cubic structure is indicated. The (111 Ni) reflection is the strongest peak, the average grain size, lattice parameter and phases with increasing Ni concentration for the alloy mainly because of the nucleation and subsequent growth rate with increasing Ni due to the difference of ionic radii of Ni and Cr ions. The plot of the X-ray diffraction data, as a spectrum, of the PD CASTA H (Co–Cr) alloy is shown in figure 4.15. The diffraction peaks are identified by (100), (002), (101), (102), (110), (103). The lattice planes indicate that the alloy has a hexagonal structure, with the (101 Co) peak the highest.

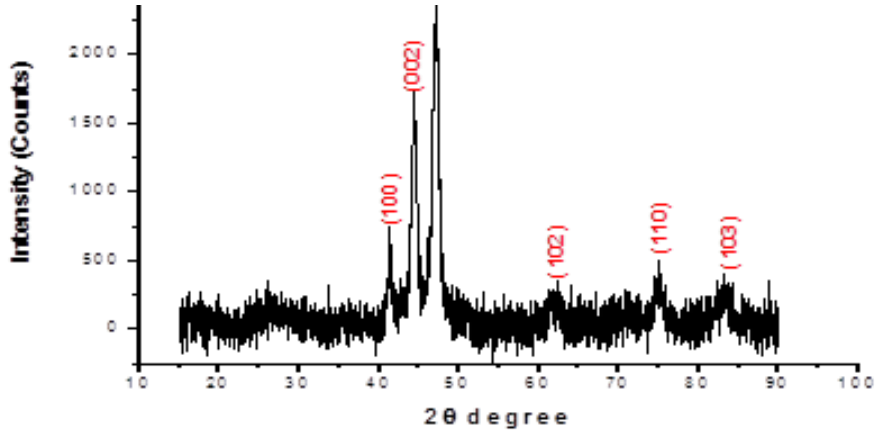

Figure 4.15: Plot of the X-ray diffraction data, as a spectrum, of the PD CASTA H (Co–Cr) alloy.

4.5 Analysis of surface roughness by Atomic Force Microscopy

AFM was used to provide three-dimensional topographic surface images in all tested alloys before and after the corrosion test. The AFM provide higher resolution than SEM. All the samples were tested and the results were shown in three-dimensional images. The difference in the surface morphology and the surface roughness from each sample were observed. The differences were based on the pH, temperatures change, composition and the immersion period. In this study, three-dimensional AFM images of the surfaces of all the tested alloys showed topographic irregularities for the alloys before and after the corrosion test.images of the surfaces of all the tested alloys showed topographic irregularities for the alloys before and after the corrosion test.

Table 4.2: Surface roughness analysis of three different dental alloys used in this study. The analysis was performed on the as is specimens and then on the specimens after immersion in Ringers solution at pH 6.5 and 37^0C, at pH 6.5 and 28^0C, at pH 6.5 and 40^0C, at pH 2.5 and 28^0C and at pH 2.5 and 40^0C.

Alloy	RMS	R_a
As is	–	–
PD CASTA H	0.022	0.014
CERACAST NB	0.021	0.122
PD 2000	0.021	0.013
pH 6.5 at 37^0C	–	–
PD CASTA H	0.106	0.031
CERACAST NB	0.170	0.025
PD 2000	0.097	0.049
pH 6.5 at 28^0C		
PD CASTA H	0.034	0.018
CERACAST NB	0.048	0.021
PD 2000	0.048	0.025
pH 6.5 at 40^0C	–	–
PD CASTA H	0.057	0.059
CERACAST NB	0.035	0.109
PD 2000	0.098	0.044
pH 2.5 at 28^0C	–	–
PD CASTA H	0.038	0.023
CERACAST NB	0.044	0.029
PD 2000	0.037	0.006
pH 2.5 at 40^0C	–	–
PD CASTA H	0.127	0.099
CERACAST NB	0.215	0.190
PD 2000	0.03	0.022

The three-dimension roughness parameter was used to quantitatively evaluate the surface topography of each alloy by using: Gwyddion–2.36 software. There were significant differences between the different alloys as showed in table 4.2. The surface topography of each alloy has been evaluated as the root mean square (RMS), average (R_a) of the distribution of heights in the AFM images. The results of using

AFM showed that there is a different in the roughness surface of the alloys before the solution test but all the alloys exhibited less roughness than that in the alloys after immersion into the corrosion test solution.. The topographic images, detailing the surface roughness of the alloys after immersion into the

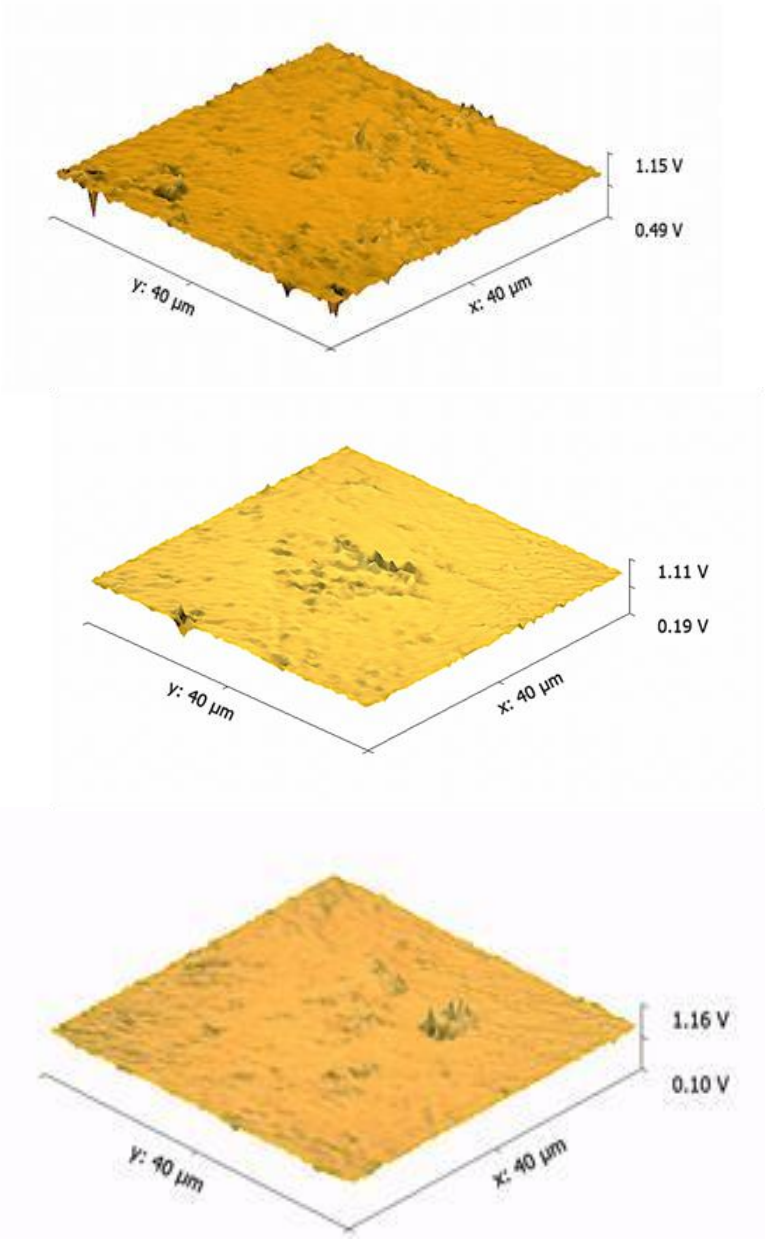

Figure 4.16: Topographic images, detailing the surface roughness of the alloys before the corrosion test by immersion into the Ringers solution. From top to bottom is shown the surface roughness of the Co–Cr–Ni alloy, Ni–Cr alloy and the Co–Cr, Ni–free alloy, as determined by Atomic Force Microscopy. The surface roughness, R_a is given in potential. An R_a of 0.1 volt corresponds to 1μm of surface roughness. The surface area scanned was $40\mu\text{m}\times40\mu\text{m}$

.

Ringers corrosion solution of pH 6.5 and temperature of 37^0C. From top to bottom is shown the surface roughness of the Co–Cr–Ni alloy, Ni–Cr alloy and the Co–Cr, Ni–free alloy, as determined by Atomic Force Microscopy are shown in figure 4.16.

The topographic images, detailing the surface roughness of the alloys after immersion into the Ringers

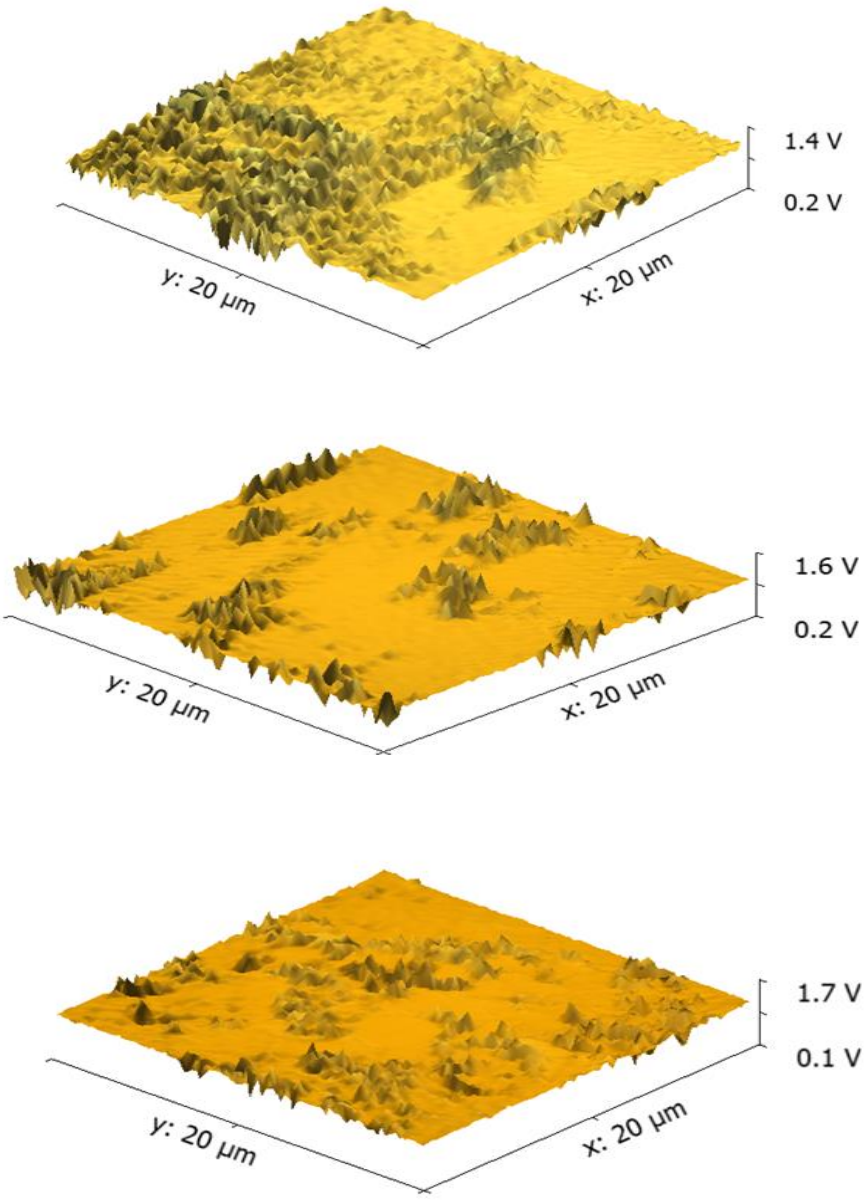

Figure 4.17: Topographic images, detailing the surface roughness of the alloys after the corrosion test by immersion into the Ringers solution of pH 6.5 and temperature of 37^0C. From top to bottom is shown the surface roughness of the Co–Cr–Ni alloy, Ni–Cr alloy and the Co–Cr, Ni–free alloy, as determined by Atomic Force Microscopy. The surface roughness, R_a is given in potential. An R_a of 0.1 volt corresponds to 1μm of surface roughness. The surface area scanned was 40μm$\times$40μm

.

corrosion solution of pH 6.5 and temperature of 28^0C. From top to bottom is shown the surface roughness of the Co–Cr–Ni alloy, Ni–Cr alloy and the Co–Cr, Ni–free alloy, as determined by Atomic Force Microscopy are shown in figure 4.17.

The topographic images, detailing the surface roughness of the alloys after immersion into the Ringers corrosion solution of pH 6.5 and temperature of 40^0C. From top to bottom is shown the surface roughness of the Co–Cr–Ni alloy, Ni–Cr alloy and the Co–Cr, Ni–free alloy, as determined by Atomic Force Microscopy are shown in figure 4.18.

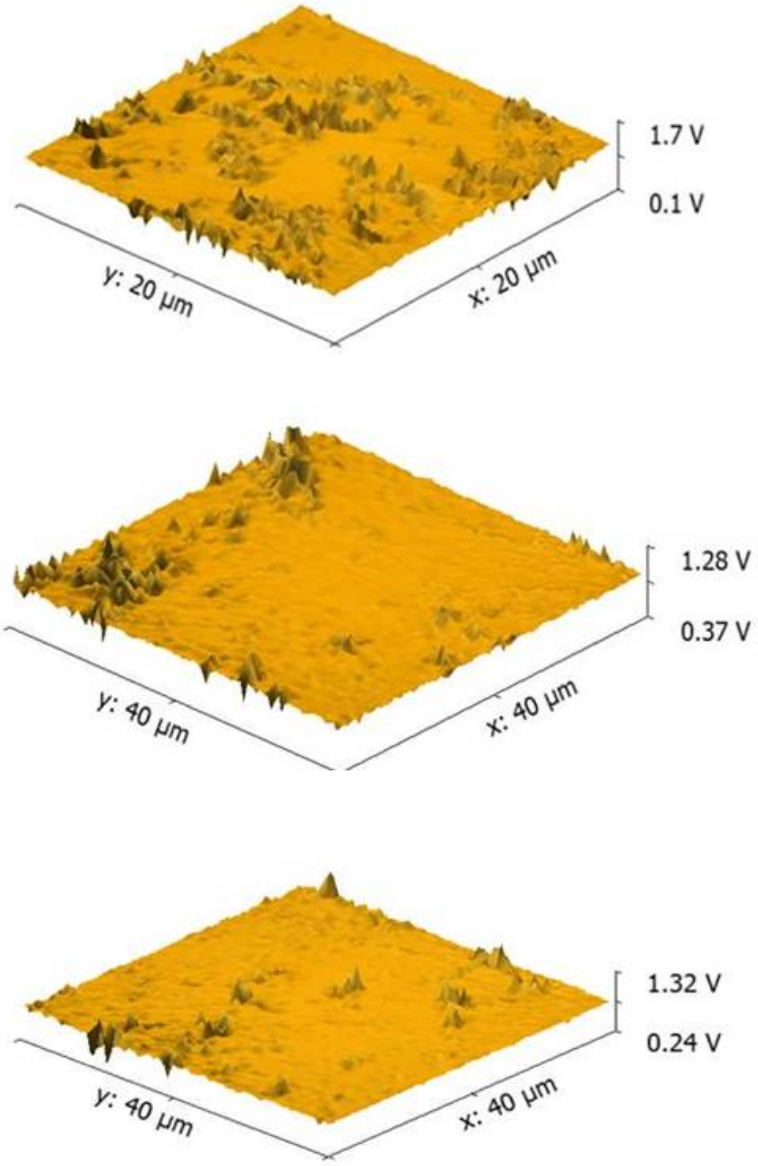

Figure 4.18: Topographic images, detailing the surface roughness of the alloys after the corrosion test by immersion into the Ringers solution of pH 6.5 and temperature of 28^0C. From top to bottom is shown the surface roughness of the Co–Cr–Ni alloy, Ni–Cr alloy and the Co–Cr, Ni–free alloy, as determined by Atomic Force Microscopy. The surface roughness, R_a is given in potential. An R_a of 0.1 volt corresponds to 1μm of surface roughness. The surface area scanned was 40μm$\times$40μm

.

The topographic images, detailing the surface roughness of the alloys after immersion into the Ringers corrosion solution of pH 2.5 and temperature of 28^0C. From top to bottom is shown the surface roughness of the Co–Cr–Ni alloy, Ni–Cr alloy and the Co–Cr, Ni–free alloy, as determined by Atomic Force Microscopy are shown in figure 4.19.

The topographic images, detailing the surface roughness of the alloys after immersion into the Ringers corrosion solution of pH 6.5 and temperature of 40^0. From top to bottom is shown the surface roughness of the Co–Cr–Ni alloy, Ni–Cr alloy and the Co–Cr, Ni–free alloy, as determined by Atomic Force Microscopy are shown in figure 4.20.

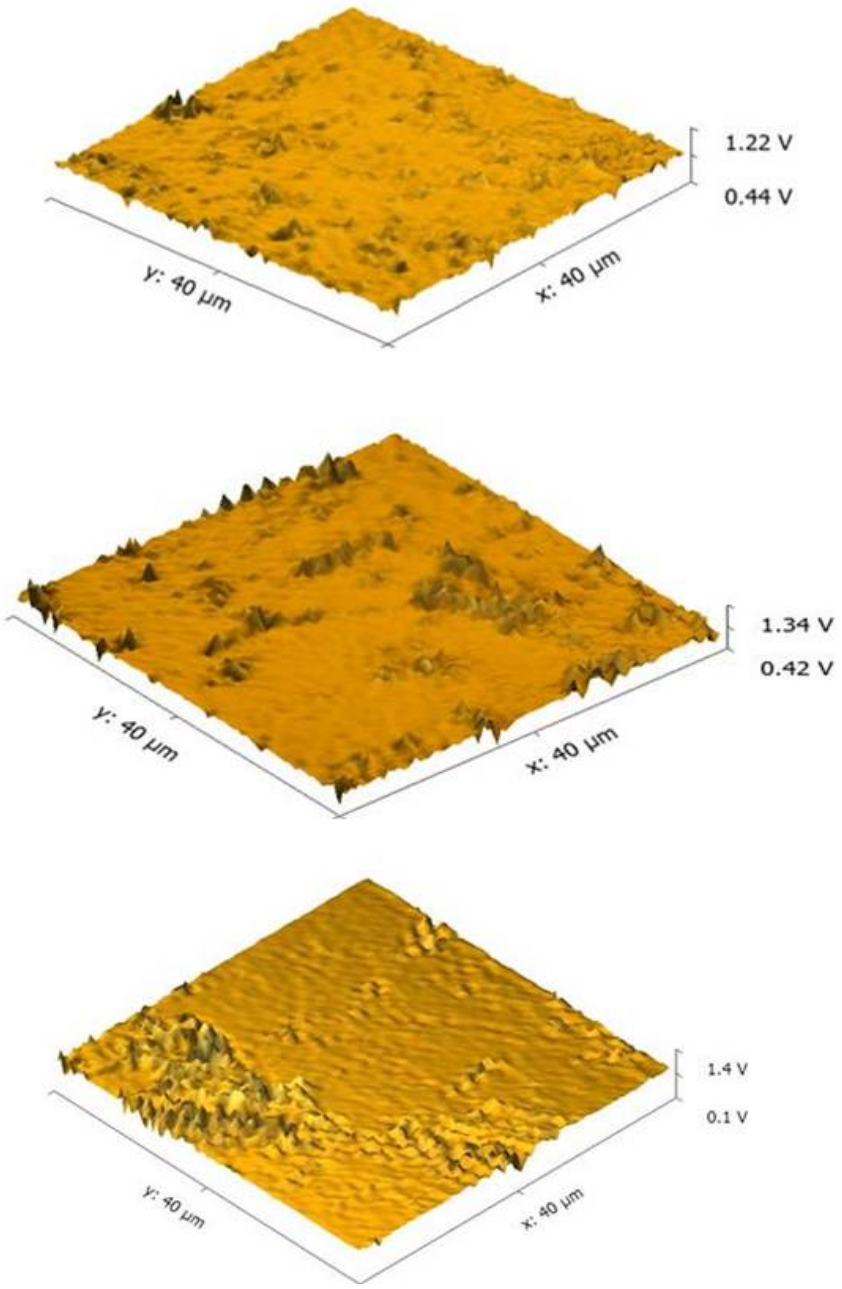

Figure 4.19: Topographic images, detailing the surface roughness of the alloys after the corrosion test by immersion into the Ringers solution of pH 6.5 and temperature of 40^0C. From top to bottom is shown the surface roughness of the Co–Cr–Ni alloy, Ni–Cr alloy and the Co–Cr, Ni–free alloy, as determined by Atomic Force Microscopy. The surface roughness, R_a is given in potential. An R_a of 0.1 volt corresponds to 1μm of surface roughness. The surface area scanned was $40\mu\text{m}\times40\mu\text{m}$

.

AFM was used to observe the surface of the dental alloys in three-dimensional images. The roughness average (Ra) and root-mean-square (RMS) of the scanned surface areas were calculated from the AFM data.

It has been understood that the dendritic surface structure of the Co–Cr, Ni–Cr alloys consist of clusters of nanocrystals which emerge from a smooth undulating and subsequently reveals characteristics of roughness. Also, there are differences in the results of all the alloys due to the scanning area size,

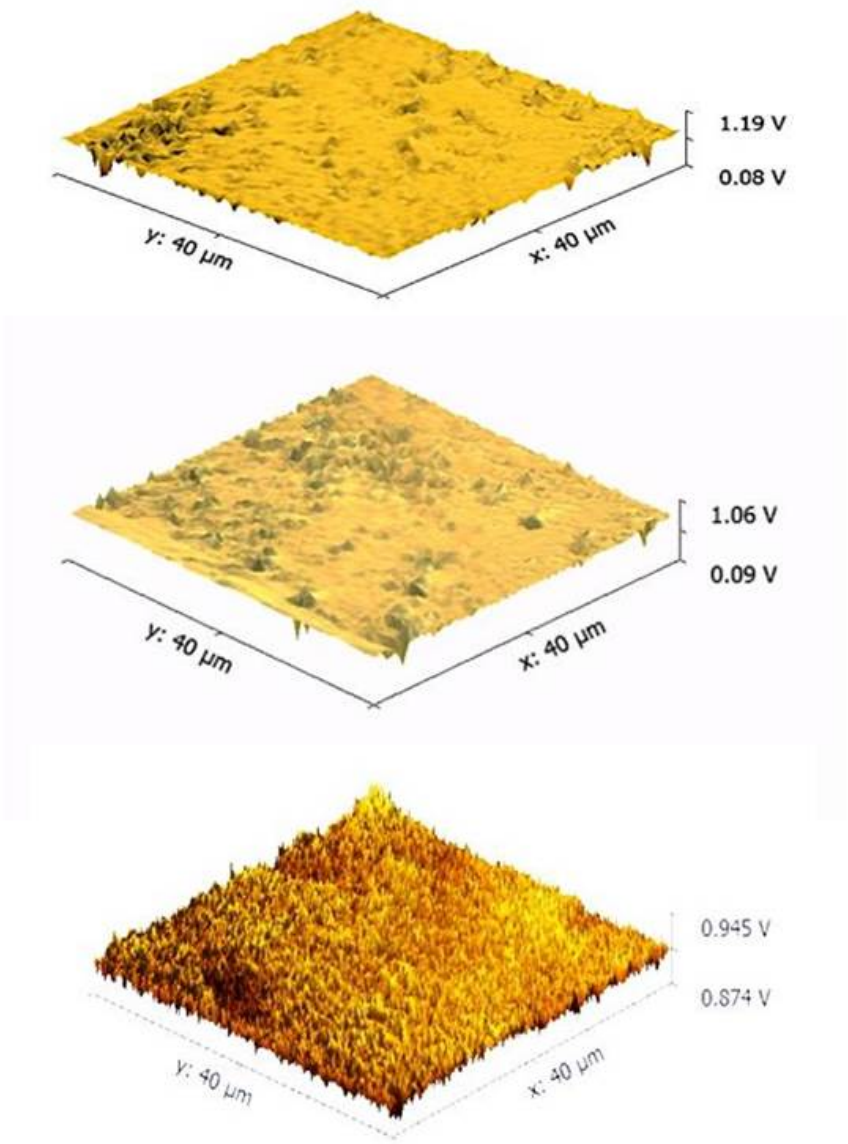

Figure 4.20: Topographic images, detailing the surface roughness of the alloys after the corrosion test by immersion into the Ringers solution of pH 2.5 and temperature of 28^0C. From top to bottom is shown the surface roughness of the Co–Cr–Ni alloy, Ni–Cr alloy and the Co–Cr, Ni–free alloy, as determined by Atomic Force Microscopy. The surface roughness, R_a is given in potential. An R_a of 0.1 volt corresponds to 1μm of surface roughness. The surface area scanned was 40μm$\times$40μm

.

although the same points were analyzed and the same experimental design used. Representative AFM–3D reconstructions for all the alloys are shown in figures above. The results shown indicates that there are less rough surfaces in the alloys before the immersion in the solution than after immersion in the Ringers corrosion solution. The comparison of mean roughness (R_a) is shown in figure 4.22.

With respect to pH, a comparison of mean surface roughness (R_a) of the alloys after the immersion into the Ringers corrosion solution at a pH of 6.5 is shown in figure 4.23.

With respect to pH, a comparison of mean surface roughness (R_a) of the alloys after the immersion into the Ringers corrosion solution at a pH of 2.5 is shown in figure 4.24.

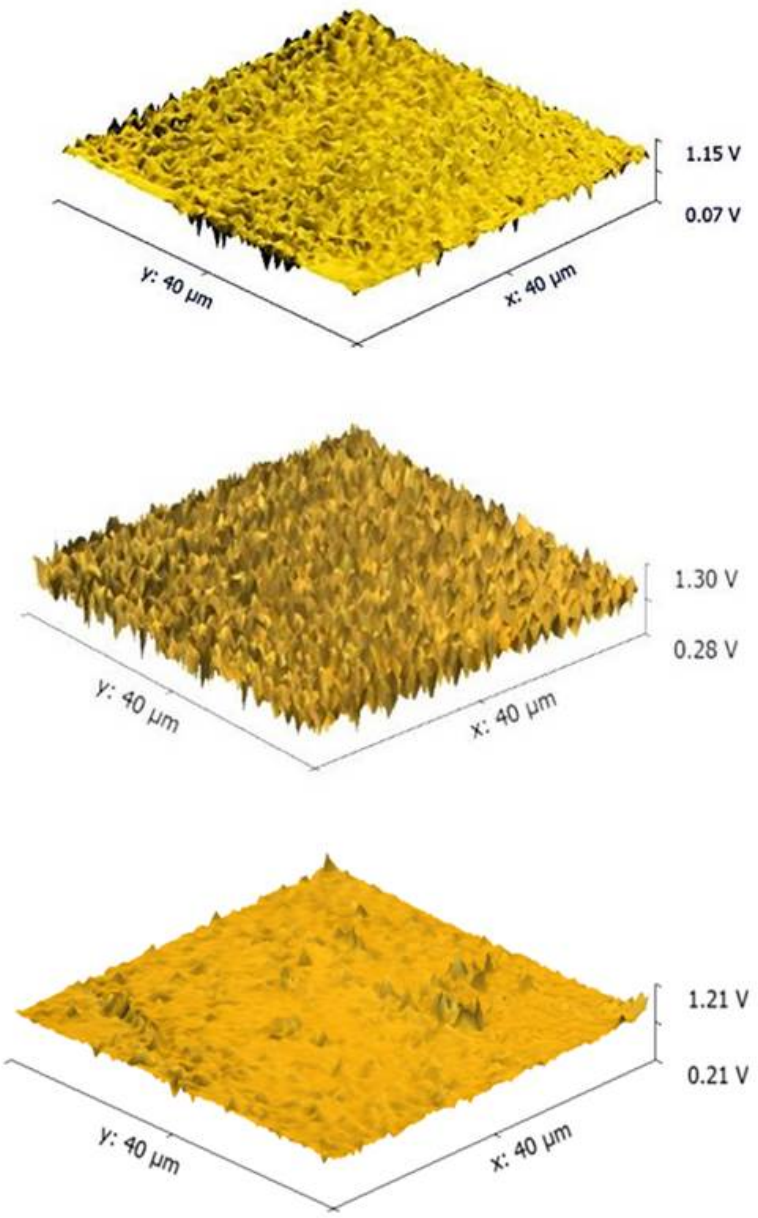

Figure 4.21: Topographic images, detailing the surface roughness of the alloys after the corrosion test by immersion into the Ringers solution of pH 2.5 and temperature of 40^0C. From top to bottom is shown the surface roughness of the Co–Cr–Ni alloy, Ni–Cr alloy and the Co–Cr, Ni–free alloy, as determined by Atomic Force Microscopy. The surface roughness, R_a is given in potential. An R_a of 0.1 volt corresponds to 1μm of surface roughness. The surface area scanned was 40μm$\times$40μm

.

4.6 Time-of-flight Secondary Ion Mass Spectrometry (TOF–SIMS)

The study was carried out using the ion TOF-SIMS, with spectroscopy: Bi^{1+}, 1pA, 10KHz (100 μs), 30 k V. The resolution was 512$\times$512 pixels, with detection limit between parts per million to parts per billion ranges, and depth profiling of less than 10nm. Samples were sputter cleaned with Cs gun for 15 seconds. The base pressure: 1.2×10^{-8} mbar. TOF–SIMS was used to analyze surface layers on CERACAST NB (Non–Precious Dental Casting Ceramic Alloy–Beryllium free), after the immersion in Ringers solution for 14 days to see the effect of the solution on the layer on the surface (see fiure 4.25. TOF–SIMS used to

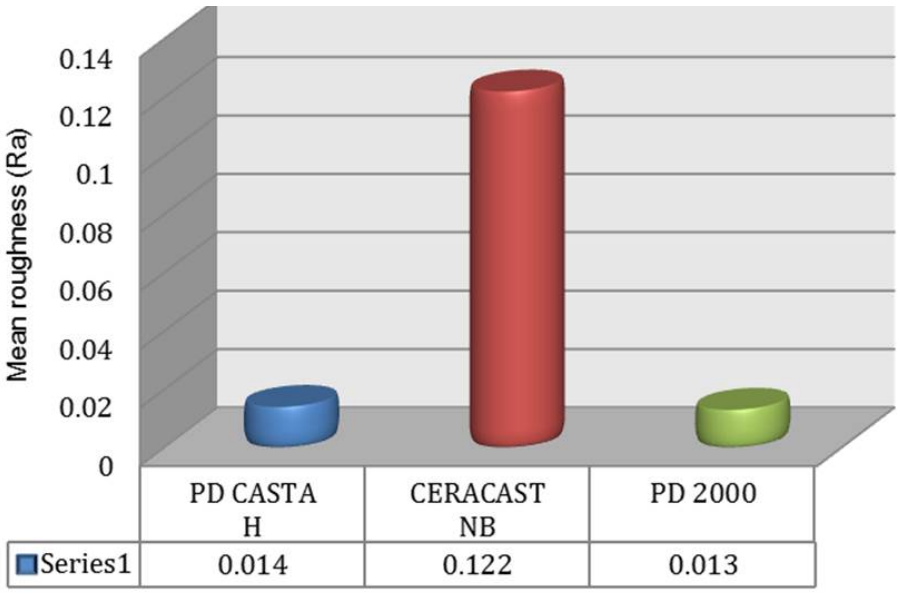

Figure 4.22: Comparison of the mean surface roughness of the three alloys before immersion into the Ringers corrosion solution.

.

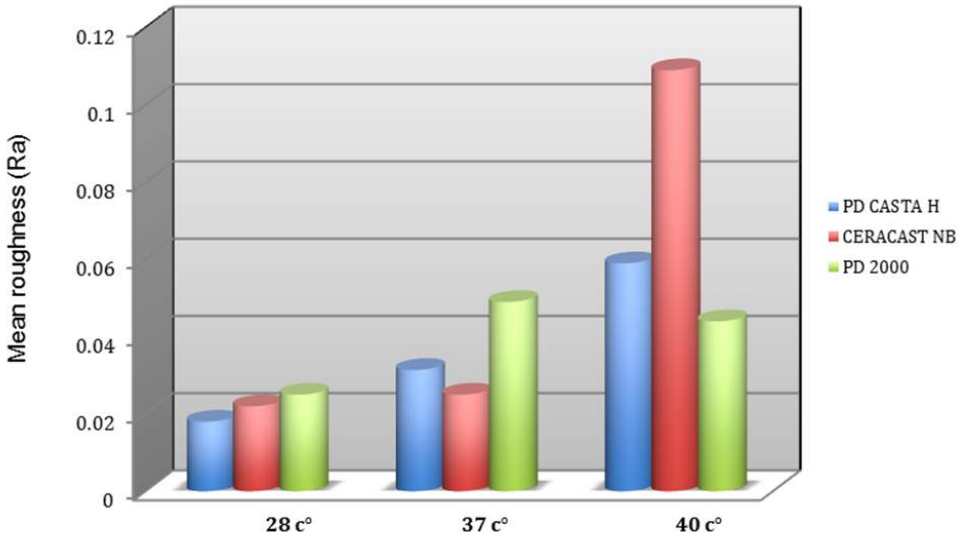

Figure 4.23: A comparison of mean surface roughness (R_a) of the alloys after the immersion into the Ringers corrosion solution at a pH of 6.5 and at the various temperatures.

got the data on the elements and phases distribution at a depth of alloy.

The most advantage of TOF–SIMS is the feasibility to image structural ions with high lateral resolution. In TOF–SIMS used, uses a pulsed Cs^+ primary ion beam to release and ionize species from a sample surface, then the resulting secondary ions are accelerated into mass spectrometer, where they are mass analyzed by measuring their time–of–flight from the sample surface to the detector. So, the secondary ions travel through the TOF analyzer with different speeds, depending on their mass to charge value. By focused beam across the surface of the alloy, the mass–imaging, elemental mapping and the images, were made by TOF- SIMS to visualize the distribution of individual species as a function of depth from the

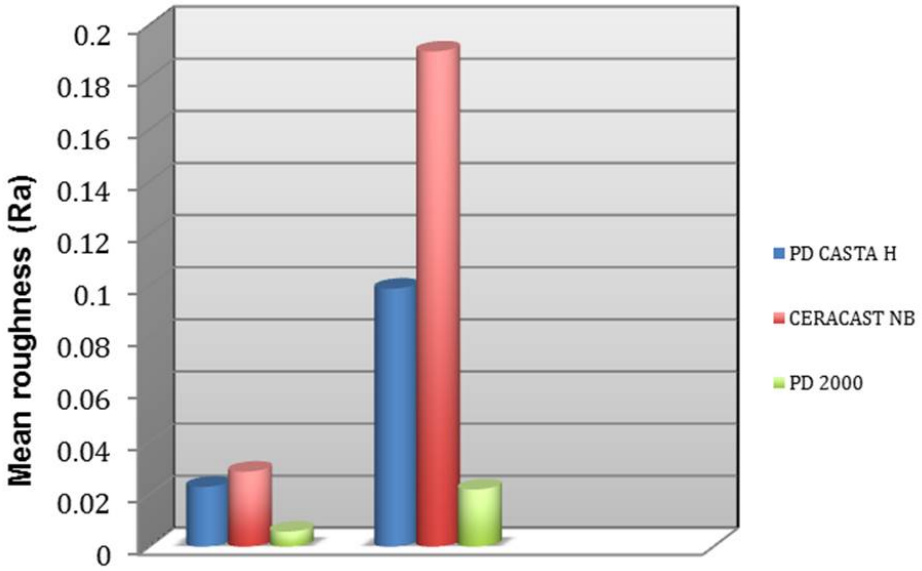

Figure 4.24: A comparison of mean surface roughness (R_a) of the alloys after the immersion into the Ringers corrosion solution at a pH of 6.5 and at the various temperatures.

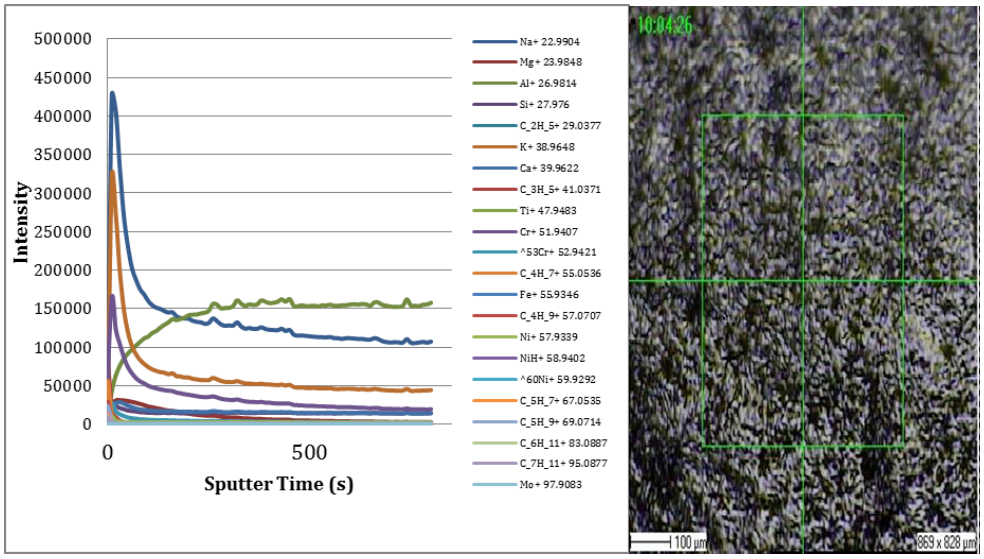

Figure 4.25: The depth profiling of concentrations of elements in the surface of the CERACAST NB alloy obtained by time–of–flight secondary ion mass spectrometry.

surface.

4.7 Summary and discussion of experimental results

Dental alloys must be more resilient to withstand the effects of most severe environment. Variations in the temperature, acidity or alkalinity value and high stresses all have an effect on the properties of materials. Normal temperature in the oral cavity is between 32^0C and 37^0C. However the acidity or alkalinity of fluids measured in the oral cavity by pH varies from around (4 to 8.5), while the intake of acid fruit juices

or alkaline medicaments can extend this range from pH 2 to 11.

The non-precious alloys react easily with the biochemical medium from the oral cavity due to their complex composition, and are especially degraded by electrochemical corrosion the selection of dental alloys depending on the mechanical and biocompatibility properties. Also on the corrosion resistance. In order to realise certain prostheses the choice of dental alloy is very important, because inadequate material may lead to mechanical, chemical or biological failures that have undesirable consequences in time for the patients general state of health (Mareci *et al.*, 2005).

The purpose of this study was to compare and examine how the dental alloys which contains Co, Cr, and Ni behaves in artificial saliva of different pH value and temperatures. This study was also envisaged to evaluate the roles of dental alloys elements and passive film homogeneity on the corrosion resistance of Co–Cr and Ni–Cr alloys. XRD experiments were carried out in order to identify the elemental and phase analysis and provides phase composition identification which determines the crystal orientation present in the microstructure of the alloys, All the peaks were different, some were sharp and other were broad. This means that if the peak is sharp, the Full Width at Half Maximum (FWHM) is small and the grain–size is large and if the peak was broad the grain–size will be small.

In this study, XRD showed that the Cr–Co alloys and Ni–Cr alloys has the mixture of large and small grains. The influence of particle size, shape and structural strain for crystalline materials has an effect on the physical and chemical properties of the dental alloys because the crystallite size can be performed by measuring the broadening of a particular X–ray diffraction (XRD) peak in a diffraction pattern. It is inversely related to the FWHM of an individual peak. The more narrow the peak, the larger the crystallite size. The results of XRD analysis indicate that the crystal structures of the tested alloys are mainly complex, sensitive to the composition of the alloys and consistent with the microstructural examinations.

In this study, SEM was used to characterize the surface morphology and the corrosion attack of the three dental alloys before and after the immersion period in artificial saliva. The SEM results for the three tested alloys in initial state showed that there is no corrosion on the surface and each sample have a different morphology. SEM showed differences in the growth of a passive oxide layer of Cr_2O_3, with small mounts of Co_3O_4, CoO and $CoCr_2O_4$ on the surfaces especially with the higher presence of Cr in the alloy. Therefore the oxide layer growth decelerates with increasing oxidation time because outward diffusion of cobalt ions is hindered by a thick, compact, and adherent oxide layer on the metal surface (Klein, 2013).

The oxidation time and the oxidation temperature have many effects in the corrosion rate, there are a higher rate constant of oxide layer when the temperatures were around 40^0C, compared to oxide layer form on other alloys at lower temperatures. The influence of different alloying elements have many affects in the oxidation process due to the variety of alloying elements which have different affinities to oxygen (Klein, 2013). The results showed that the corrosion resistance of the Ni–Cr alloys is related to the formation of passive film containing $Ni(OH)_2$, NiO, Cr_2O_3 and MoO_3 on the surfaces. The presence

of Ni in the oxide film is also important in metal protection. In most Cr–Co alloys, which has a maximum of about 20 to 25% of Cr, a layer of Cr_2O_3 forms on the alloy surface. The Cr content is the key alloying addition determining passive film stability, which improve hot corrosion properties. The presence of a substantial Mo content (9%) is required to achieve maximum film stability. A higher content of Cr_2O_3 and MoO_3 in the passive film could lead to a higher resistance to metal ion transfer through the passive film. The homogeneous distribution of Cr is critical especially in low–Cr nickel–based alloys for better corrosion resistance compared with Cr_2O_3. The oxide of nickel is more porous and has less protective ability to corrosion. Hence, the passive film zones, which are rich in NiO, will act as weak regions for localized corrosion, which can cause localized dissolution of Ni–rich phases (Silva *et al.*, 2011). In contrast, silicon enhances the oxidation resistance not only because of SiO_2 formation but also due to the beneficial effect of silicon on the formation of protective Al_2O_3 (Sato *et al.*, 2011).

Lactic acid will ionize to lactate and H^+ ion, when this acid added to the Ringers corrosion solution. The ionization process of lactic acid is due to a decrease in the pH value on the solution. Therefore the corrosion resistance decrease when the lactic acid addition on the solution. On other hand the pH also decrease with increasing the amount of lactic acid. The corrosion rate is therefore aggravated with an increase in lactic acid. In the present study, topographic surface characteristics of the three alloys were evaluated by AFM. The AFM was used to provide three-dimensional topographic surface images before and after the corrosion test and provide higher resolution images. All the alloys were tested and the results were shown in three–dimensional image. Therefore, AFM is recommended for the quantitative analysis of surfaces of the alloys with nano–scale irregularities. The different in the surface morphology and the surface roughness from each sample were observed. The differences were based on the pH values, temperatures change, composition and the immersion period.

In this study, TOF–SIMS experiments were carried out for the alloy CERACAST NB (Non–Precious Dental Casting Ceramic Alloy–Beryllium Free), after the immersion in Ringers solution. This ultrahigh vacuum surface analytical system used to study surface structure, composition, and chemical state by means of secondary ion detection during ion sputtering. The capabilities include surface spectroscopy with high sensitivity and mass resolution, surface imaging with high lateral resolution, depth profiling with high depth resolution and 3D analysis. In general the corrosion rate increases with increasing temperature because of changes in the temperature inside the mouth due to consuming different foods and liquids at varying temperatures, it may be effect on corrosion resistance of dental alloys.

From this study there is a decrease in corrosion resistance with increasing temperature of the solution. This may be because the oxygen concentration in the solution decreased. However, in an acid solutions when the pH is fixed at 2.5, the corrosion rate will be increased with increases in temperature, due to the hydrogen release. However the corrosion rate increases with increasing temperature only until the temperature becomes high enough to cause decrease in the oxygen solubility. Alkaline salts hydrolyze to increase solution pH. This may act as corrosion inhibitors. Some common alkaline salts are trisodium

phosphate, sodium tetraborate, sodium silicate, and sodium carbonate. Oxidizing salts such as ferric chloride, cupric chloride, and sodium hypochlorite are especially corrosive to carbon steel. Oxidizing salts that are inhibitors include Na_2CrO_4, $NaNO_2$, and $KMnO_4$. The homogeneous distribution of Cr is critical especially in low–Cr nickel–based alloys for better corrosion resistance. Compared with Cr_2O_3, the oxide of nickel is more porous and has less protective ability to corrosion. Hence, the zones of passive film rich in NiO will act as weak regions for localized corrosion, which causes localized dissolution of Ni–rich phases. There is a current trend of replacing Ni–Cr alloys, commonly used as dental ceramic, with Co–Cr alloys, because of its more expected biocompatibility.

CHAPTER 5

Conclusions and Recommendations

5.1 Conclusions

The main objective of this study was to evaluate the corrosion resistance of three different dental alloys on artificial saliva solution of various pH values and temperatures. However, it was concluded that the pH and temperatures of the solution had effects on the corrosion of dental alloys.

The following were concluded based on the structural optical and physical properties of the dental alloys:

- The alloys have a well-defined crystallographic structure,
- The presence of crevices combined with an inhomogeneous distribution of Cr in the microstructure can lead to accelerated corrosion of alloys with lower Cr contents,
- The corrosion resistance was depended on the chemical composition of dental alloys, and immersion period that each alloy took. However it is important to know the biocompatibility of different metal ions in dental alloys to avoid allergic or some other diseases during fixed or denture treatment on the teeth,
- The surface and optical properties of the alloys were studied by AFM, in form of three-dimensional imaging. It was observed that the dendritic surface structure of the Co–Cr, Ni–Cr alloys consists of clusters of nanocrystals which emerge from a smooth undulating surface that reveals characteristics regarding roughness. Therefore smooth surface of the alloys is very important as they determine the area of the contact surface with fluids in the oral cavity, The surface layers of the alloys was studied after corrosion test using TOF–SIMS gave the distribution profile and the secondary ion emission spectra of surface layer in one nanometer resolution,

- The overall corrosion resistances were observed for the alloys with content of Co and Cr. This is due to the passivation phenomenon attributed to the formation of a protective layer of chromium oxide, thus inhibiting the corrosion process, and
- In general, the good corrosion resistance of the Cr–Co, and Ni–Cr alloys in Ringers solution is due to the highly protective passive oxide film that is the key factor for its compatibility.

5.2 Recommendations

The present study tested three different dental alloys used in dental application, to determine how the mechanical properties and biocompatibility are affected inside the oral cavity. However, based on the finding of this study, the following are recommended:

1. In vitro studies are needed to determine the chemical composition and the biological application of the alloys,
2. A report of this need to be carefully documented because any change in any one of the parameters, albeit the chemical materials used, the oral temperatures and the pH may lead to inconsistent results,
3. All the results suggest that the use of non–precious alloys have high corrosion resistance and Co–Cr alloys exceed corrosion resistance compared to the other alloys containing Ni–Cr in artificial saliva, and
4. On the basis of the results obtained, our advice would be to recommend to avoid an increase in the oral temperature and avoid the taking of acid food which are probably to lower the pH of the oral cavity and increase the corrosion of the alloys when the removable or fixed partial dentures treatment.

CHAPTER 6

REFERENCES

Agrawal, C. 1998. Reconstructing the human body using biomaterials. *Journal of the Minerals, Metals and Materials Society*, vol. 50(1), pp. 31–35.

Al Subari, R. Bellaouchou, A., Guenbour, A. & Merzouk, N. 2013. Influence of temperature and pH on corrosion behavior of Ni–Cr and Co–Cr dental alloys. *Journal of International Dental and Medical Research*, vol. 6(1), pp. 9–14.

Alkmina, L.B., Silvaa, A.A.P., Nunes, C.A., Santos, C. & Coelho, G.C. 2014. Microstructural evidence of beryllium in commercial dental Ni–Cr alloys. *Materials Research,* vol. 17(3), pp. 627–631.

American Dental Associatoon (ADA). 1972. Guide to dental materials and devices: *Specification no. 5 for dental casting gold alloy*. 6th Edition, Chicago.

Anusavice, K.J. 1996. *Phillips' Science of Dental Materials.* 2nd Edition. WB Saunders, Philadelphia, USA.

Anusavice, K.J. 2003a. Informatics systems to assess and apply clinical research on dental restorative materials. *Advances in Dental Research*, vol. 17(1), pp. 43–48.

Anusavice, K.J. 2003b. *Phillips' Science of Dental Materials.* 11th Edition. Saunders & Elsevier Science, University of Michigan, United States of America.

Anusavice, K.J. 2006. *Phillips' Science of Dental Materials*. 11th Edition. Saunders, Philadelphia, USA.

Ardakani, F. E., Davari, A., Goodarzipour, D., Goodarzipour, K. & Fallahzadeh, H. 2004. Evaluation of the diagnostic of intra–oral D and E film for detecting interproximal caries. *The Journal of Contemporary Dental Practice*, vol. 5(4), pp.58–70.

Atlas of Dental Ceramics. *Volume II–Bridge Design and Laboratory Procedures in Dental Ceramics*. Quintessence, Chicago, USA.

Awan, M. 2010. *A study investigating the mechanical testing of a novel dental restorative material and its biocompatibility.* MSc Dissertation, University of Birmingham, Birmingham. United Kingdom.

Axelsson, P. 2000. *Diagnosis and risk prediction of dental caries*. 1st Edition. Quintessence.

Aziz–Kerrzo, M.C.K., Fenelon, A.M., Farrell, S.T. & Breslin, C.B. 2001. Electrochemical studies on the stability and corrosion resistance of titanium–based implant materials. *Biomaterials,* vol. 22, pp. 1531–1539.

Badawy, W.A., El–Rabie, M.M., Helal, N.H. & Nady, H. 2010. Corrosion Inhibition of Mg–Al–Zn alloy in neutral chloride solutions. *Corrosion Science*, vol. 55(24), pp. 1880–1887.

Bard, A.J. & Faulkner, L,R. 2001. *Electrochemical Methods: Fundamentals and Applications*. 2nd Edition. John Wiley & Sons, University of Texas, Austin, USA.

Barsoukov, E. & Macdonald, J.R. 2005. *Impedance Spectroscopy–Theory, Experiment and Applications*. 2nd Edition. John Wiley & Sons Inc, Hoboken, New Jersey, USA.

Bennani, A., Amine, A. & Eladioui, S. 2008. Etude électrochimiques des alliages Ni–Cr utilisés en prothèse fixée. *Cahier Prothése*, vol. 143, pp.63–71.

Bergman, M.B., Bergman, R. & Söremark, J. 1980. Tissue accumulation of nickel released due to electrochemical corrosion of non–precious dental casting alloys. *Journal of Oral Rehabilitation,* vol. 7(4), pp. 325–330.

Berstein, A., Bernauer, I., Marx, R. & Geurtsen, W. 1992. Human cell culture studies with dental metallic materials. *Biomaterials*, vol. 13(2), pp. 98–100.

Binnig, G., Quate, C.F. & Gerber, C. 1986. Atomic force microscope. *Physical Review Letters*, vol. 56(9), pp. 930–933.

Brand, R.W. & Isselhard, D.E. 2003. *Anatomy of Orofacial Structures*. 6th Edition. Mosby, Missouri, USA.

Brandon, D. & Kaplan, W.D. 2008. *Microstructural Characterization of Materials*. 2nd Edition. Wiley, London, UK.

Bumgardner, J.D. & Lucas, L.C. 1993. Surface analysis of nickel chromium dental alloys. *Dental Materials*, vol. 9(4), pp. 252–259.

Castner, D.G. & Ratner, B.D. 2002. Biomedical surface science: Foundations to frontiers. *Surface Science*, vol. 500(1), pp. 28–60.

Charng, T. & Lansing, F. 1982. Review of corrosion causes and corrosion control in a technical facility. *The Telecommunications and Data Acquisition Progress Report 42–69*, Code: 311–034191, pp. 145–156.

Craig, R.G. 1997. *Restorative Dental Materials.* 10th Edition. Mosby, University of Sydney Library, Sydney, Australia.

Craig, R.G., O'Brien, W.J. & Powers, J.M. 1983. *Dental Materials, Properties and Manipulation*. 5th Edition. Mosby–Year Book, New York, USA.

Cremasco, A., Osorio, W.R., Freire, C.M.A., Garcia, A. & Caram, R. 2008. Electrochemical corrosion behavior of a Ti–5Nb alloy. *Electrochimica Acta*, vol. 53(14), pp. 4867–4874.

Cullity, B.D. 1978. *Elements of X–Ray Diffraction*. 2nd Edition. Addison–Wesley Publishing Company. University of Notre Dame, Indiana, USA.

De Almeida, P.D.V., Grégio, A.M.T., Machado, M.Â.N., de Lima, A.A.S. & Azevedo, L.R. 2008. Saliva composition and functions: A comprehensive review. *The Journal of Contemporary Dental Practice*, vol. 9(3), pp. 72–80.

Dong, H., Nagamatsu, Y., Chen, K.K., Tajima, K., Kakigawa, H., Shi, S. & Kozono, Y. 2003. Corrosion behavior of dental alloys in various types of electrolyzed water. *Dental Materials Journal*, vol. 22(4),

pp. 482–493.

Douglas, C.H. 2008. Metal corrosion in the human body: The ultimate bio–corrosion scenario. *The Electrochemical Society Interface*, vol. 17(2), pp. 31–34.

Evans Analytical Group (EAG). *The worldś leading fully integrate independent laboratory network*. Avaliable online at: (www.EAGLABS.com).

Fifield F.W. & Kealey D. 2000. *Principle and Practice of Analytical Chemistry*. 3rd Edition. Blackwell Science, London, UK.

Finne, K., Göransson, K. & Winckler, L. 1982. Oral lichen planus and contact allergy to mercury. *International Journal of Oral Surgery,* vol. 11(4), pp. 236–239.

Fischer, J. 2002. Effect of small additions of Ir on properties of a binary Au—Ti alloy. *Dental Material*, vol. 18(4), pp. 331–335.

Frelich, M.A. & Meriers, J.C. 2004. Fiber–reinforced composite prostheses. *Dental Clinics of North America*, vol. 48(2), pp. 545–562.

Geis–Gerstorfer, J. & Passler, K. 1993. Studies on the influence of Be content on the corrosion behavior and mechanical properties of Ni–25Cr–10Mo alloys. *Dental Materials*, vol. 9(3), pp. 177–181.

Geurtsen, W. 1994. Metallic restorations as an alternative to amalgam. *Deutsche Zahnärztliche Zeitschrift*, vol. 49, pp. 853–858.

Geurtsen, W. 2002. Biocompatibility of dental casting alloys. *Critical Reviews in Oral Biology and Medicine*, vol. 13(1), pp. 71–84.

Gil, F.J., Sánchez, L.A., Espías, A. & Planell, J.A. 1999. *In vitro* corrosion behavior and metallic ion release of different prosthodontics alloys. *International Dental Journal,* vol. 49(6), pp. 361–367.

Gosser, D. K. 1993. *Cyclic Voltammetry: Simulation and Analysis of Reaction Mechanisms*. VCH Publishers, Wiley, New York, USA.

Grimsdottir, M.R. & Hensten–Pettersen, A. 1993. Cytotoxic and antibacterial effects of orthodontic appliances. *Scandinavian Journal of Dental Research*, vol. 101(4), pp. 229–231.

Henriques, B., Soares, D. & Silva, F.S. 2012. Microstructure, hardness, corrosion resistance and porcelain shear bond strength comparison between cast and hot pressed Co–Cr–Mo alloy for metal–ceramic dental restoration. *Journal of the Mechanical Behavior of Biomedical Materials*, vol. 12, pp. 83–92.

Heyrovsky J. & Zuman P. 1968. *Practical Polarography; An Introduction for Chemistry Students*. Academic Press, New York, USA.

Huang, H.H. 2002a. Effect of chemical composition on the corrosion behavior of Ni–Cr–Mo dental casting alloys. *Journal of Biomedical Materials*, vol. 60(3), pp. 458–465.

Huang, H.H. 2002b. Effects of fluoride concentration and elastic tensile strain on the corrosion resistance of commercially pure titanium. *Biomaterials*, vol. 23(1), pp. 59–63.

Humphrey, S.P. & Williamson, R.T. 2001. A review of saliva: normal composition, flow, and function. *Journal of Prosthetic Dentistry*, vol. 85(2), pp. 162–169.

Hung, P.I. 2008. *Oral health care performance for in–patients among nurses at Hanoi City Hospital, Vietnam*. MSc Dissertation. Mahidol University, Bangkok, Thailand.

Hussain, S. 2008. *Investigation of Structural and Optical Properties of Nanocrystalline ZnO*, MSc Dissertation, Linkoping University, Sweden.

Jenkins, G.N. 1985. *The Physiology and Biochemistry of the Mouth*. J.B. Lippincott Company of Canada. 4th Edition. Blackwell Scientific Publications, Toronto, Canada.

Johansson, B.I., Hao, S.Q. & Lemons, J.E. 1989a. Corrosion of dental copper, nickel and gold alloys in artificial saliva and saline solutions. *Dental Materials Journal*, vol. 5(1), pp. 324–328.

Johansson, B.I., Lucas, L.C. & Lemons, J.E. 1989b. Corrosion of copper, nickel, and gold dental casting alloys: an *in vitro* and *in vivo* study. *Journal of Biomedical Materials*, vol. 23(A3 Suppl), pp. 349–361.

Karina, A.N.O., Maximiliano, P.N., Paulo, C.R. & Marco, A.B. 2004. Mechanical properties and microstructure analysis of a Ni–Cr alloys cast under different temperatures. *Brazillian Journal of Oral*

Sciences, vol. 3(8), pp. 414–419.

Kelly, J.R. 1997. Ceramics in restorative and prosthetic dentistry. *Annual Review of Materials Science,* vol. 27(1), pp. 443–468.

Klein, A. 2013. *High Temperature Oxidation and Electrochemical Studies on Novel Co–base Superalloys*. PhD Dissertation, Universitat Erlangen, Nurnberg, Germany.

Knosp, H., Holliday, R.J. & Corti, C.W. 2003. Gold in dentistry: Alloys, uses and performance, *Gold Bulletin*, vol. 36(3), pp. 93–102.

Koike, M. & Fujii, H. 2001. *In vitro* assessment of corrosive properties of titanium as a biomaterial. *Journal of Oral Rehabilitation,* vol. 28(6), pp. 540-–548.

Koike, M., Nakamura, S. & Fujii, H. 1997. *In vitro* assessment of release from titanium by immersion tests. *The Journal of the Japan Prosthodontic Society*, vol. 41(4), pp. 675–679.

Kovacevic, N., Pihlar, B., Selih, V.S. & Milocev, I. 2012. The effect of pH value of a simulated physiological solution on the corrosion resistance of orthopaedic alloys. *Acta Chimica Slovenia,* vol. 59(1), pp. 144–155.

Kumar, S. & Narayanan, S. 2008. Corrosion behavior of Ti—15Mo alloy for dental implant applications. *Journal of Dentistry*, vol. 36(7), pp. 500–507.

Langer, R. 1999. Biomaterials in drug delivery and tissue engineering: One laboratory's experience. *Accounts of Chemical Research*, vol. 33(2), pp. 94–101.

Lawrence, G.W. & Marshall, K.W. 1999. *Health Promotion Planning: An Educational and Ecological approach*. 3th Edition. Mayfield Publishing Company, Ann Arbor, USA.

Lawson, J.R. 1991. Alternative alloys for resin–bonded retainers. *Journal of Prosthetic Dentistry,* vol. 65(7), pp. 97–99.

Lucas, L.C., Dale, P., Buchanan, R., Gill, Y., Griffin, D. & Lemons, J.E. 1991. *In vitro* vs *in vivo* corrosion analyses of two alloys. *Journal of Investigative Surgery*, vol. 4(1), pp. 13–21.

Mabilleau, G., Bourdon, S., Joly–Guillou, M.L., Filmon, R., Baslé, M.F. & Chappard, D. 2006. Influence of fluoride, hydrogen peroxide and lactic acid on the corrosion resistance of commercially pure titanium. *Acta Biomaterialia*, vol. 2(1), pp. 121–129.

Mansfeld, F. 1976. *Advances in Corrosion Science and Electrochemical Techniques for Technology.* 6th Edition. Plenum press, New York, USA.

Maoela, M.S. 2009. *Spectro–electrochemical determination of the antioxidant properties of Carpobrotus mellei and Carpobrotus quadrifidus natural products*. PhD Dissertation, University of the Western Cape, Bellville, South Africa.

Mareci, D., Nemtoi, G.H., Aelenei, N. & Bocanu, C. 2005. The electrochemical behaviour of various non–precious Ni–Co based alloys in artificial saliva. *European Cells and Materials*, vol. 10(8), pp. 1–7.

Martin, Y., Williams, C.C. & Wickramasinghe, H.K. 1987. Atomic Force Microscopy–force mapping and profiling on a sub 100 scale. *Journal of Applied Physic*s, vol. 61(10), pp. 4723–4729.

Masatoshi, T., Masafumi, K. & Yukyo, T. 2011. Corrosion behavior of Ti–Ag alloys used in dentistry in lactic acid solution. *Metal and Materials International*, vol. 17(1), pp. 175–179.

Massler, M. 1967. Pulpal reaction to dentinal caries. *International Dental Journal*, vol. 17(2), pp. 441–460.

McCabe, J.E. & Walls, A.W.G. 2008. *Applied Dental Materials*. 9th Edition. Blackwell Sciences, Oxford, UK.

Mohammad, H.H. 2014. *Electrochemical Behavior of some Metals of Technological Importance in aqueous solutions*. MSc Dissertation, Fayoum University, Cairo, Egypt.

Morris, H.F. 1987. Veterans administration cooperative study project No 147, part IV. Biocompatibility of base metal alloys. *Journal of Prosthetic Dentistry*, vol. 58(1), pp.1–5.

NATIONAL INSTITUTE OF DENTAL RESEARCH (NIDR). 1984. Workshop: Biocompatibility of metals in dentistry. *The Journal of the American Dental Association*, vol. 109(3), pp. 469–471.

Nimmo, B. & Hinds, G. 2003. *Beginners Guide to Corrosion.* NPL's Corrosion Group from various source material, pp. 1–10.

Ornberg, A. 2007. *Study of Electrochemical Behaviour and Corrosion Resistance of Materials for Pacemaker Lead Applications.* Licentiate Thesis, Royal Institute of Technology, Stockholm, Sweden.

Peterson, D. 2001. Dental caries circles of infection diseases, family gentle dental care. *Oral Care Report*, vol. 10(4).

Philips, R. W. 1991. *Science of Dental Materials*. 9th Edition. W.B. Saunders, Philadelphia, USA.

Philips, R.W. & Skinner, E.W. 1965. *Elements of dental materials*. 8th Edition. W.B. Saunders, Philadelphia, USA.

Powers, J.M. & Sakaguchi, R.L. 2006. *Craig's Restorative Dental Materials*, 12th Edition. Mosby/Elsevier, Portland, Oregon, USA.

Qing, Q.U., Lei, W., Yajun, C., Lei, L., Yue, H. & Zhongtao, D. 2014. Corrosion behavior of titanium in artificial saliva by lactic acid. *Materials Journal*, vol. 7(8), pp. 5528–5542.

Raghavan, V. 1981. *Materials Science and engineering–A first course.* Prentice–Hall of India Private Limited, New Delhi, India.

Rana, D.S., Chaturvedi, D.K. & Quamara, J.K. 2009. Morphology, crystalline structure, and chemical properties of 100MeV Ag–ion beam irradiated polyvinylidene fluoride (PVDF) thin film. *Journal of Optoelectronics and Advanced Materials*, vol. 11(5), pp. 705–712.

Reed, S.J.B. 2005. *Electron Microprobe Analysis and Scanning Electron Microscopy in Geology*. Cambridge University Press, New York, USA.

Robert, B. 1995. *Corrosion tests and standards–application and interpretation,* Chapter 7, American Society for Testing and Materials (ASTM).

Rosentiel, S.F., Land, M.F. & Fujimoto, J. 1995. *The metal–ceramic crown preparation.* In Contemporary Fixed Prosthodontics. 2nd Edition. Mosby–year book, St. Louis, USA.

Russell, R. & Yiming, L. 1998. *In vitro* evaluation of biocompatibility of experimental titanium alloys for dental restorations. *Journal of Prosthetic Dentistry*, vol. 80(4), pp. 495–500.

Samson, E., Lemaire, G., Marchand, J. & Beaudoin, J.J. 1999. Modeling chemical activity effects in strong ionic solutions. *Computational Materials Science*, vol. 15, pp. 285–294.

Sato, A., Chiu, L. & Reed, R.C. 2011. Oxidation of nickel–based single–crystal superalloys for industrial gas turbine applications. *Acta Materialia,* vol. 59(1), pp. 225–240.

Schiff, N., Grosgogeat, B., Lissac, M. & Dalard, F. 2002. Influence of fluoride content and pH on the corrosion resistance of titanium and its alloys. *Biomaterials*, vol. 23(9), pp.1995–2002.

Schmalz, G., Arenholt–Bindslev, D., Pfüller, S. & Schweikl, H. 1997. Cytotoxicity of metal cations used in dental cast alloys. *ATLA*, vol. 25(2), pp. 323–330.

Schmalz. G. & Garhammer, P. 2002. Biological interaction of dental cast alloys with oral tissues. *Journal of Dental Materials*, vol. 18(5), pp. 396–406.

Sharma, M.A.V., Kumar, R. & Singh, N. 2008. Electrochemical corrosion behaviour of dental/ implant alloys in saline medium. *The Journal of Materials Science*, vol. 19(7), pp. 2647–2653.

Silva, J.W.J., Sousa, L.L., Nakazato, Z.R., Codaro, N.A. & Felipe, H. 2011. Electrochmical and microstructure study of Ni–Cr–Mo alloys in dental prostheses. *Materials Science and Application*, vol. 2(1), pp. 43–48.

Smith, A.J. 2002. Pulpal responses to caries and dental repair. *Caries Research*, vol. 36(4), pp. 223–232.

Stamenkovic, D., Cairovic, A.L., Colic, M., Rudolf, R., Radovic, K. & Dorđevic, I. 2009. The effect of repeated casting on the biocompatibility of a dental gold alloy. *Acta Veterinaria* (Beograd), vol. 59 (5–6), pp. 641–652.

Stephan, T. 2001. TOF–SIMS in cosmochemistry. *Planetary and Space Science*, vol. 49(9), pp. 859–906.

Sun, D., Monaghan, P., Brantley, W.A. & Johnston, W.M. 2002. Potentiodynamic polarization study of the *in vitro* corrosion behavior of 3 high–palladium alloys and a gold–palladium alloy in 5 media. *The Journal of Prosthetic Dentistry*, vol. 87(1), pp. 86–93.

Sutow, E.J., Jones, D.W. & Milne, E.L. 1985. *In nitro* Cre Cele vice corrosion behaviour of implant materials. *Journal of Dental Research*, vol. 64, pp. 842–847.

Tafforeau, M., Claire Verdus, M., Norris, V., White, G., Demarty, M., Thellier, M. & Ripoll, C. 2002. SIMS study of the calcium–deprivation step related to epidermal meristem production induced in flax by cold shock or radiation from a GSM telephone. *Journal of Trace and Microprobe Techniques*, vol. 20(4), pp. 611–623.

Tenovuo, J., Lagerlof, F., Thylstrup, A. & Fejerskov, O. 1994. *Textbook of Clinical Cariology*. 2nd Edition. Munksgaard, Copenhagen, Denmark.

Van Noort, R. 2002. *Introduction to Dental Materials,* 3rd Edition. Mosby Wolfe. London, UK.

Wang, J. 2000. *Analytical Electrochemistry*. 3rd Edition. WILEY–VCH, New York, USA.

Wang, R.R. & Yiming, L. 1998. *In vitro* evaluation of biocompatibility of experimental titanium alloys for dental restorations. *Journal of Prosthetic Dentistry*, vol. 80(4), pp. 495–500.

Wataha, J.C. 2000. Biocompatibility of dental casting alloys, a review. *Journal of Prosthetic Dentistry,* vol. 83(2), pp. 223–234.

Wataha, J.C., Craig, R.G. & Hanks, C.T. 1991. The release of elements of dental casting alloys into cell–culture medium. *Journal of Dental Research*, vol. 70(6), pp. 1014–1018.

William, A. & Satish, B. 2012. Metallurgy – Advances in materials and processes/heat treatment of dental alloys: A Review. *InTech*, University of Birmingham, Birmingham, UK.

Williams, D. 1981. *Biomaterials an Biocompatibility: An introduction, in Fundamental Aspects of Biocompatibility*, CRC press, Boca Raton.

Yamamoto, A., Honma, R. & Sumita, M. 1998. Cytotoxicity evaluation of 43 metal salts using murine fibroblasts and osteoblastic cells. *Journal of Biomedical Materials Research*, vol. 39(2), pp. 331–340.

Zanello, P. 2003. *Inorganic Electrochemistry: Theory, Practice and Application*. The Royal Society of Chemistry, London, UK.